Circulation Research

Check for updates

ORIGINAL RESEARCH

BAHCC1 Drives Smooth Muscle Plasticity and Neointima via Epigenetic Repression

Runze Tang, Yitao Huang, Takuro Shirasu, Jing Li, Amy Webb, Kaiyuan Zheng, Chengli Shen, Yiran Guo, Gaelle Auguste, Patrick Hart, Maria Murach, Xinyu Zhou, Jianjie Ma, K. Craig Kent, Gang Greg Wang, Jie Yang, Clint L. Miller, Kathleen Ann Martin, Lian-Wang Guo

BACKGROUND: Vascular smooth muscle cell (SMC) phenotypic plasticity drives neointimal hyperplasia (IH) and contributes to atherosclerosis. Epigenetic mechanisms have been implicated in SMC plasticity, but the roles of epigenetic reader proteins are poorly understood. BAHCC1 (bromo adjacent homology domain coiled-coil 1) is a newly identified reader of the gene-repression histone mark histone-3 lysine 27 trimethylation (H3K27me3). Its role in vascular remodeling is unknown.

METHODS: We investigated BAHCC1 in human restenotic and atherosclerotic arteries and in rat and mouse arterial injury models using BAHCC1 silencing, SMC-specific deletion, and an H3K27me3-binding-deficient knock-in mutation. Mechanistic studies in human aortic SMCs integrated transcriptomic and epigenomic profiling, protein-interaction assays, and single-guide RNA-dCas9-based epigenetic editing.

RESULTS: BAHCC1 was upregulated in human restenotic and atherosclerotic arteries and rat arteries with IH. While BAHCC1 silencing reduced IH in balloon-injured rat arteries, SMC-specific BAHCC1 deletion and the H3K27me3-binding-deficient mutation (BAHCC1^{Y2537A}) attenuated IH in wire-injured mouse arteries. In human SMCs, mitogen induced BAHCC1 expression through nuclear factor Y subunit-α, promoting BAHCC1-dependent dedifferentiation. Integrated transcriptomics and epigenomics identified LMO7 (LIM domain only 7), an IH suppressor, as a key BAHCC1-repressed target. BAHCC1 occupancy at *LMO7* required BAHCC1-H3K27me3 interaction, and *LMO7*-targeted H3K27me3 enrichment through epigenetic editing repressed its expression in a BAHCC1-dependent manner. Furthermore, BAHCC1 associated with SAP30 and RBBP4/7 to form a corepressor complex. Functionally, LMO7 silencing reversed the effects of BAHCC1 knockdown on human SMC phenotype and exacerbated IH in BAHCC1^{Y2537A} mice. Human genetic analyses further identified BAHCC1 variants associated with cardiovascular phenotypes and BAHCC1 expression.

CONCLUSIONS: BAHCC1 is a previously unrecognized epigenetic driver of vascular remodeling. By reading H3K27me3 and recruiting corepressors to repress gene expression, BAHCC1 promotes pathological SMC phenotypic transition and IH, highlighting the BAHCC1 pathway as a potential therapeutic target for IH-associated vascular disease.

GRAPHIC ABSTRACT: A graphic abstract is available for this article.

Key Words: chromatin reader ■ phenotypic transition ■ restenosis ■ SAP30 ■ vascular remodeling

Circulation Research FIRST PROOF ONLY

Downloaded from http://ahajournals.org by on November 5, 2026

Atherosclerosis remains a leading cause of morbidity and mortality worldwide. Common interventions, such as angioplasty and bypass grafting, aim to restore blood flow but are often compromised by restenosis due to neointimal hyperplasia (IH).[1] This pathological response contributes to adverse outcomes, including heart failure and stroke. In the United States, the only approved anti-restenotic therapies are drug-eluting stents and drug-coated balloons.[2] However, these interventions have limitations, including in-stent restenosis, potential stent thrombosis and mortality, the requirement for dual antiplatelet therapy, reduced effectiveness in complex or bifurcated lesions, and limited efficacy in patients with diabetes and peripheral vascular disease.[3–6]

Correspondence to: Lian-Wang Guo, Department of Surgery, School of Medicine, University of Virginia, 409 Ln Rd, Charlottesville, VA 22903. Email lg8zr@virginia.edu
Supplemental Material is available at https://www.ahajournals.org/doi/suppl/10.1161/CIRCRESAHA.126.329470.
© 2026 American Heart Association, Inc.
Circulation Research is available at www.ahajournals.org/journal/res

Downloaded from http://ahajournals.org by on November 5, 2026

Novelty and Significance

What Is Known?

- Vascular smooth muscle cell (SMC) plasticity is epigenetically regulated and central to occlusive vascular pathologies, including neointimal hyperplasia (IH) and atherosclerosis.
- Histone mark histone-3 lysine 27 trimethylation (H3K27me3) is a repressive histone modification implicated in IH, but how this epigenetic mark is interpreted mechanistically in SMCs remains poorly understood.
- The bromo adjacent homology-domain protein BAHCC1 (bromo adjacent homology domain coiled-coil 1) is a recently discovered H3K27me3 reader, but its role in vascular disease is unknown.

What New Information Does This Article Contribute?

- BAHCC1 is induced in vascular SMCs after arterial injury and promotes pathological SMC plasticity and IH.
- SMC-specific deletion of BAHCC1 or mutational disruption of its H3K27me3-reader function attenuates IH, supporting a functional role for BAHCC1-H3K27me3 reading in vascular remodeling.
- BAHCC1 assembles a SAP30-RBBP4/7 corepressor complex to repress target gene expression, including the IH suppressor LMO7 (LIM domain only 7), which mediates the effects of BAHCC1 on SMC plasticity and IH.

SMC plasticity is epigenetically regulated and central to vessel-narrowing IH in many occlusive vascular pathologies. However, how gene-repressive histone modifications are interpreted to control SMC phenotype remains poorly understood. This study identifies BAHCC1, a recently discovered reader of the repressive histone mark H3K27me3, as a previously unrecognized regulator of pathological SMC plasticity and IH. Using SMC-specific knockout and knock-in mouse models, we show that BAHCC1 in SMCs and its ability to read H3K27me3 promote IH following arterial injury. Mechanistically, BAHCC1 translates H3K27me3 into gene repression by forming a complex with corepressors SAP30 and RBBP4/7 to silence genes that restrain pathological SMC transition. Among these targets, LMO7, an IH suppressor, mediates the effects of BAHCC1 on SMC plasticity and vascular remodeling, revealing a repression-of-suppressor mechanism in IH. Thus, our study uncovers a previously unrecognized mechanism linking H3K27me3 reading by BAHCC1 to pathological SMC plasticity and identifies the BAHCC1 pathway as a potential therapeutic target for IH-associated vascular disease.

FIRST PROOF ONLY

Nonstandard Abbreviations and Acronyms

BAHCC1	bromo adjacent homology domain coiled-coil 1
CUT&Tag	cleavage under targets and tagmentation
CVD	cardiovascular disease
H3K27me3	histone-3 lysine 27 trimethylation
HAoSMC	human aortic SMC
IH	neointimal hyperplasia
LMO7	LIM domain only 7
NFYA	nuclear transcription factor Y subunit alpha
sgRNA	single-guide RNA
SMC	vascular smooth muscle cell
WT	wild-type

Thus, there is an urgent need for alternative therapeutic strategies to prevent restenosis.

Unlike terminally differentiated striated muscle cells, vascular smooth muscle cells (SMCs) possess remarkable phenotypic plasticity that allows for adaptive vascular remodeling but also contributes to IH. IH is a complex process of vascular wall remodeling involving multiple cell types, including vascular cells and immune cells, with SMC phenotypic changes playing a predominant role in injury-induced IH.[7–9] During this process, SMCs transition from a contractile to a dedifferentiated state, acquiring proliferative, migratory, and ECM (extracellular matrix)-producing properties that lead to neointima formation that can occlude the lumen.[10] This pro-IH SMC phenotypic transition is fundamentally driven by epigenetic regulation.[11] Injury-induced disruptions in the vascular wall microenvironment precipitate distinct histone modifications. The reversibility of these epigenetic modifications underlies the reversible phenotypic plasticity of SMCs, and suggests promising targets for novel, safe therapies.[12] However, epigenetic mechanisms underlying SMC plasticity and IH are incompletely understood.

Histone H3 lysine-27 trimethylation (H3K27me3) is a histone mark that regulates gene repression, epigenetic memory, and cell fate transition.[13] Although DNA methylation and histone acetylation states have been extensively studied in the context of IH,[14–17] the role of H3K27me3 in IH development is not well understood.[18, 19] H3K27me3 is deposited by PRC2 (polycomb repressive complex 2), with the methyltransferase

component being EZH2 (enhancer of zeste homolog 2) or a related homologous enzyme, EZH1[20]. Readers (effectors) that recognize H3K27me3, such as chromo domain-containing CBX proteins, were previously reported to mediate the establishment and spreading of so-called polycomb domains in the genome[20]. Most recently, BAHCC1 (bromo adjacent homology domain coiled-coil 1), a scarcely studied protein, was discovered to be a specific reader that binds H3K27me3 directly through its evolutionarily conserved bromo adjacent homology protein module[21]. BAHCC1 is highly upregulated in human cancers, including hematologic cancer and certain solid tumors[20-22], promoting proliferation and metastasis[21]. The role of BAHCC1 in the vasculature is completely unknown, but we hypothesized that it may be implicated in IH, a proliferative pathology. We and others have previously shown that pharmacological reduction of H3K27me3, the histone modification ligand of BAHCC1, attenuates IH[18, 19, 23]. In this study, we explored the role of BAHCC1 in SMCs and identified a role in IH pathogenesis and downstream target genes that modify SMC phenotypic plasticity.

METHODS

Data Availability

Data have been made publicly available at the NCBI Gene Expression Omnibus (GSE346675, GSE347071) or from the corresponding author upon reasonable request.

Formalin-Fixed, Paraffin-Embedded Human Artery Tissue Sections

Formalin-fixed, paraffin-embedded sections were purchased from CVPath Institute (Gaithersburg, MD). Restenosis sections were taken from coronary arteries 5 mm within stent ends, and control sections were from nonrestenotic locations. Atherosclerotic sections were derived from coronary arteries, and control sections were from healthy aortic samples. All samples were deidentified.

Generation of SMC-Specific BAHCC1 Knockout Mice

All animal studies conformed to the Guide for the Care and Use of Laboratory Animals (National Institutes of Health, 2011, eighth edition). All animal procedures were approved by the University of Virginia Animal Care and Use Committee. The BAHCC1 floxed mouse line was generated by GemPharmatech Co., Ltd (San Diego). The knockout region comprises exons 10 to 13 of *Bahcc1*. *Myh11-CreER^{T2}-RAD* mice[24] were purchased from The Jackson Laboratory (strain 037658). *Bahcc1$^{flox/flox(f/f)}$* mice were crossed with *Myh11-CreER^{T2}-RAD* mice to obtain *Bahcc1$^{f/f}$*; *Myh11-CreER^{T2}-RAD* mice. This new line is inducible for SMC-specific BAHCC1 knockout (BAHCC1^{iSMCKO}). To induce BAHCC1^{iSMCKO}, 13- to 14-week-old male or female *Bahcc1$^{f/f}$*; *Myh11-CreER^{T2}-RAD* mice were fed tamoxifen diets (Inotiv, TD.130860) for 10 days at a dose of 40 mg/kg body weight, followed by a 7-day washout period before surgery. Littermate *Bahcc1$^{f/f}$* mice were used for the control group, which received tamoxifen treatment identical to that of the *Bahcc1$^{f/f}$*; *Myh11-CreER^{T2}-RAD* group. All mice were genotyped by PCR amplification using DNA extracted from mouse ear samples. The specific primers for genotyping are listed in the Major Resources Table. Western blot analysis of aortic protein lysates was performed to confirm BAHCC1 deletion.

Wire Injury of Mouse Femoral Arteries

Wire-mediated vascular injury was performed as we described previously[25]. In brief, the major procedures were as follows: anesthetize the mouse with isoflurane through a closed-circuit anesthetic apparatus, then place the mouse in a supine position with the left hindlimb slightly abducted; make a 1.5-cm straight, longitudinal skin incision on the left medial thigh from the knee joint to the groin; under a dissecting microscope, after looping the superficial femoral artery, common femoral artery, and deep femoral artery, make a small opening in the deep femoral artery with microscissors, then insert a 0.015-inch guidewire through the opening and leave the wire inside for 1 minute. The wire was removed, and the arteriotomy site was ligated with a 7-0 suture. The skin incision was closed with a 6-0 silk suture.

For in vivo gene knockdown, 1×10^9 transduction units per mL of shRNA-LMO7 (LIM domain only 7) or shRNA-Scramble lentivirus dispersed in a 30% Pluronic gel solution were applied perivascularly to the wire-injured femoral artery segments. To maximize in vivo transduction efficiency, a single dose of 1×10^8 transduction units per mL, 100 µL of shRNA-LMO7 or shRNA-Scramble lentivirus was administered by tail vein injection the next day. To avoid bias in morphometric analysis, 1 mouse that showed complete stenosis 28 days after shRNA-LMO7 delivery was excluded.

Targeted Epigenetic Editing Through CRISPR-dCas9

To modulate H3K27me3 levels site-specifically at the LMO7 gene, we used a CRISPR-dCas9 (deactivated Cas9) system. The single-guide RNA (sgRNA) sequences were designed using CRISPick from the BROAD Institute (https://portals.broadinstitute.org/gppx/crispick/public), targeting the LMO7 promoter region (transcription start site −1500 to transcription start site +300). The best sgRNAs were determined as the top-ranked sequences based on factors including on-target and off-target scores. To generate sgRNA expression vectors, each pair of oligonucleotides (sequences as below) was annealed into double-stranded DNA and then cloned into the pLenti-sgRNA vector (Addgene 71409), which had been digested with BsmBI (New England Biolabs) and gel-purified. The pLenti-sgRNA vector without an sgRNA sequence (empty vector) was used as the sgRNA control. The constructs were then transformed into Stable Competent *E coli* (New England Biolabs) for expansion. Plasmids were extracted using the Plasmid Plus Midi Sample Kit (QIAGEN) after proper insertion was confirmed. The dCas9 plasmid (Addgene 110823), and dCas9-EZH2 plasmid (Addgene 122375) were obtained from Addgene. The plasmids were transfected into HEK293T cells using Lipofectamine 2000 reagent (Thermo Fisher Scientific) following the

Circulation Research FIRST PROOF ONLY

Downloaded from http://ahajournals.org by on November 5, 2026

manufacturer's instructions. After 48 hours, expression of the dCas9-EZH2 fusion protein was detected by Western blot using an anti-EZH2 antibody (CST).

Statistical Analysis

Data were analyzed using GraphPad Prism 8.0 and R software (version 4.4.3). Quantitative data were expressed as mean ± SEM. The statistical testing strategy was predetermined based on the sample size per group (n). For groups with n≥10, the Shapiro-Wilk test was first used to assess data normality. If the normality assumption was met, parametric tests were applied: the Student *t* test was used for 2-group comparisons, and ANOVA was used for multigroup comparisons. For sample sizes of n<10 or when the data deviated from a normal distribution, nonparametric methods were strictly executed. The Mann-Whitney *U* test was performed for 2-group comparisons. For multigroup evaluations, a Kruskal-Wallis test followed by the Benjamini-Krieger-Yekutieli post hoc correction was implemented for 1-way analysis, whereas a 2-way aligned rank transform ANOVA followed by the Holm post hoc test was applied for multifactor designs. Two-sided $P<0.05$ indicated statistical significance, and all *P* values or adjusted *P* values are explicitly displayed on the corresponding graphs. Multiple testing corrections were not applied globally across different experiments. Statistical adjustments were performed strictly within each individual test. No multiple samples or tissue sections were taken from the same animal for the statistical analyses. Each individual data point (N) represents a completely independent sample derived from a distinct animal.

RESULTS

BAHCC1 Is Upregulated in the Diseased IH-Bearing Arteries of the Human or Rat Origin

We and others have previously shown upregulation of H3K27me3 in rat arteries undergoing IH, and that its reduction by an EZH inhibitor mitigated IH[18, 19, 23]. Consistently, our immunofluorescence analysis revealed a marked increase in H3K27me3 levels in human restenotic arteries compared with nonrestenotic controls (Figure 1A). Interestingly, immunofluorescence also illustrated substantial upregulation of BAHCC1 in human restenotic and atherosclerotic artery samples compared with the respective control samples (Figure 1B and 1C; representative hematoxylin and eosin staining shown in Figure S1). These data link BAHCC1 to human vascular pathology. Given that BAHCC1 is a specific reader of H3K27me3,[21] we hypothesized that BAHCC1 might play a role in IH.

We then examined the modulation of BAHCC1 expression in a rat carotid artery injury model of IH, which mimics balloon angioplasty injury in human arteries. Dual immunofluorescence staining revealed induction of BAHCC1 in αSMA-positive SMCs after arterial injury, with its expression increasing as early as day 3, reaching a maximum at day 7, and remaining significantly elevated through day 14 relative to uninjured arteries (Figure 1D). These results together link upregulation of BAHCC1 to the pathophysiology of IH.

IH Is Attenuated Either by BAHCC1 Knockdown in Injured Rat Arteries or by SMC-Specific BAHCC1 Knockout in Injured Mouse Arteries

To investigate the role of BAHCC1 in the development of IH, we first performed BAHCC1 knockdown in rat carotid arteries using the balloon angioplasty model[26-28]. To express BAHCC1-specific shRNA or scrambled shRNA control, lentivirus was intraluminally applied and then locally infused into the injured artery wall immediately after angioplasty. Immunofluorescence confirmed effective BAHCC1 knockdown compared with scrambled shRNA controls (Figure S2). Morphometric analysis indicated that IH was reduced in BAHCC1-shRNA arteries, as measured by the intima area normalized either to the medial area (neointima/media area ratio) or to the IEL perimeter (neointimal thickness) at 14 days post-angioplasty (Figure 2A). Accordingly, the stenosis rate was reduced by ≈50% as well. The EEL perimeter was not altered, indicating no reduction in the outer diameter of the vessel compared with the scrambled control (Figure 2A).

While multiple cell types contribute to injury-induced IH, SMCs are central drivers of the pathology[7-9]. Dual immunofluorescence staining indicated that BAHCC1 was predominantly expressed in αSMA-positive SMCs in injured rat arteries (Figure 1D). In contrast, BAHCC1 did not colocalize with the endothelial marker CD31 in injured arteries where the endothelium was denuded (Figure S3), indicating that BAHCC1 expression is largely confined to SMCs after vascular injury. We thus next investigated the SMC-specific role of BAHCC1 using the mouse femoral artery wire-injury model, which is well-established for studying IH[25, 29] (Figure 2B). We generated a novel *Myh11-CreER^{T2}-RAD; Bahcc1$^{fl/fl}$* line and confirmed that SMC-specific BAHCC1 knockout was induced after tamoxifen treatment in adult mice (Figure S4). Consistent with our findings in the rat artery angioplasty model (Figure 2A), inducible BAHCC1 deletion in SMCs reduced IH by ≈50% compared with BAHCC1^{WT} (*Bahcc1$^{fl/fl}$*) littermate controls (Figure 2C). Stenosis was similarly attenuated, with no change in EEL perimeter. To rigorously validate the specificity of this phenotype, we analyzed 3 genetic control groups: tamoxifen-treated *Myh11-CreER^{T2}-RAD* mice, tamoxifen-treated *Bahcc1$^{fl/fl}$* mice, and *Myh11-CreER^{T2}-RAD; Bahcc1$^{fl/fl}$* mice maintained on a normal diet (Figure S5). No significant difference in IH was observed among these control groups, confirming that the protective phenotype observed in inducible SMC-specific BAHCC1 knockout (BAHCC1^{iSMCKO}) male mice is specifically attributable to tamoxifen-induced deletion of BAHCC1 in SMCs rather than nonspecific effects of

Downloaded from http://ahajournals.org by on November 5, 2026

Circulation Research FIRST PROOF ONLY

Downloaded from http://ahajournals.org by on November 5, 2026

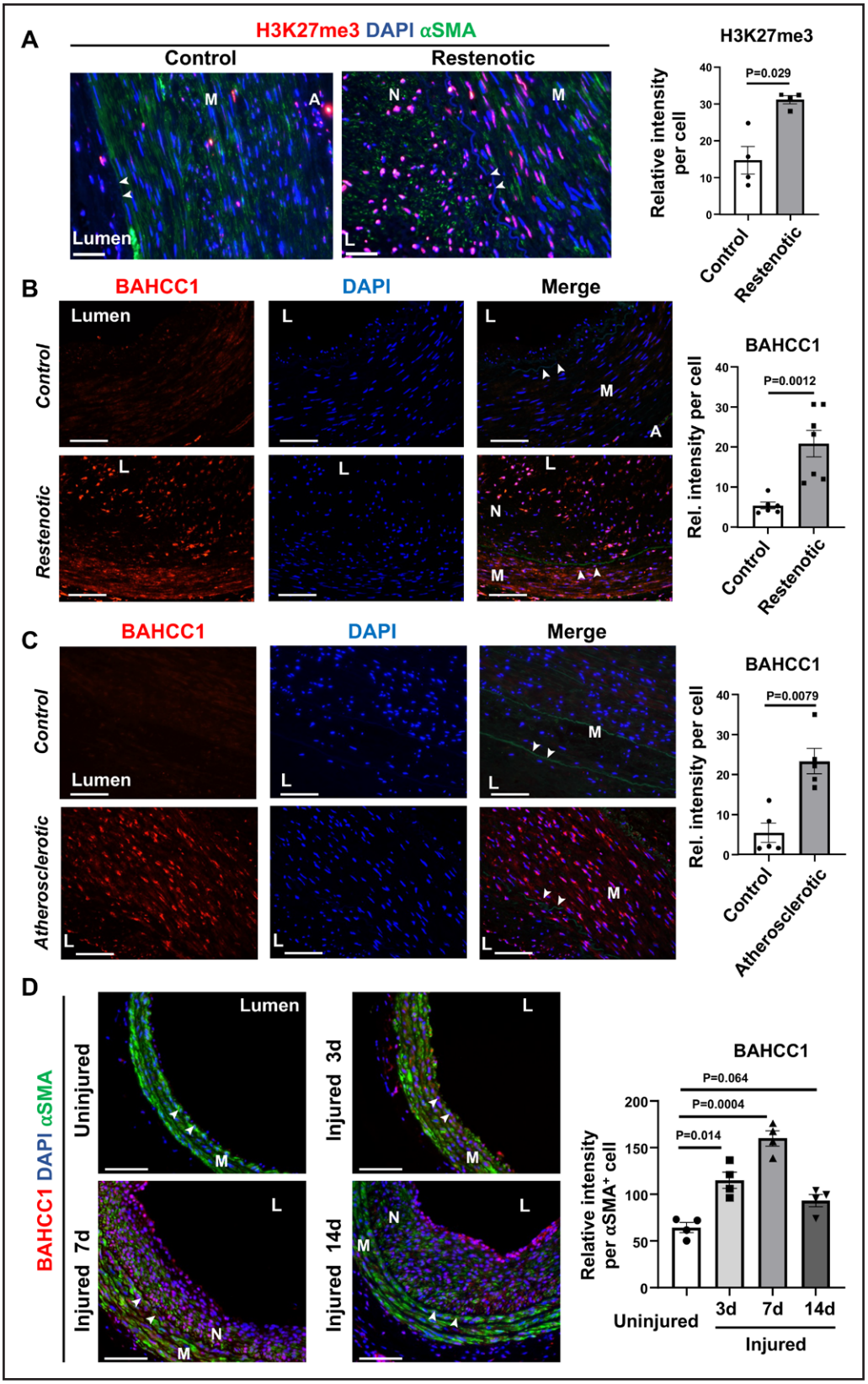


Figure 1. Upregulation of BAHCC1 (bromo adjacent homology domain coiled-coil 1) in human and rat diseased artery tissues. **A**, Histone-3 lysine 27 trimethylation (H3K27me3; red) and αSMA (green) immunostaining in human coronary restenotic arteries and nonrestenotic controls. Scale bar: 50 μm. Quantification: n=4 patients; Mann-Whitney *U* test. **B**, BAHCC1 (red) immunostaining in human coronary restenotic arteries and nonrestenotic controls. Green: elastic laminae autofluorescence. Scale bar: 100 μm. Quantification: n=6 or 7 patients; Mann-Whitney *U* test. **C**, BAHCC1 (red) immunostaining in human coronary atherosclerotic arteries and healthy aortic (*Continued*)

the Cre driver, tamoxifen treatment, or the floxed allele. Moreover, the IH-mitigating effect was also observed in female mice, in which BAHCC1^{iSMCKO} mice similarly developed less IH than female BAHCC1^{WT} controls (Figure S6), consistent with the protective effect observed in male mice. Together, these genetic studies in mice establish BAHCC1 in SMCs as a key driver of IH following arterial injury.

Disruption of the BAHCC1-H3K27me3 Reader-Mark Dyad Mitigates IH

BAHCC1 is a multidomain large protein[21, 30], and its H3K27me3-independent functions have been reported[22, 31]. We thus next investigated whether the H3K27me3-reader function of BAHCC1 contributes to IH development. To this end, we used a mouse line carrying the Y2537A mutation (BAHCC1^{Y2537A}; Figure S7), which disrupts the direct binding of the BAH domain of BAHCC1 (BAHCC1^{BAH}) with H3K27me3[21] (see the schematic in Figure 3A). In the femoral artery wire-injury model, BAHCC1^{Y2537A} mice showed markedly reduced neointima/media area ratio, neointimal thickness, and stenosis rate compared with wild-type (WT) controls (Figure 3B and 3C). These changes were similar in magnitude to the effects of SMC-specific knockout of BAHCC1 (Figure 2). There was no change in EEL perimeter. These results demonstrate that the pro-IH activity of BAHCC1 is largely mediated through its H3K27me3-binding BAH domain.

BAHCC1 Modulates the Pro-IH Pathobiology of SMCs In Vitro, and Its Expression Is Regulated by Nuclear Transcription Factor Y Subunit Alpha

Phenotypic modulation of SMCs, the major cellular component of the tunica media, is well documented to play a pivotal role in IH pathogenesis[32, 33]. PDGF (platelet-derived growth factor) is released from platelets recruited to sites of vascular injury, and PDGF-BB treatment of SMCs in culture recapitulates the phenotypic transitions that lead to IH. PDGF-BB is a mitogen known to potently induce SMC phenotypic transition characterized by dedifferentiation (reduced SMC marker expression) and enhanced cell proliferation and ECM protein synthesis in vitro[34]. As shown in Figure 4A, BAHCC1 was upregulated by PDGF-BB stimulation in human aortic SMCs (HAoSMCs). To determine the functional significance of this upregulation, we silenced BAHCC1 using shRNA. BAHCC1 knockdown increased contractile proteins MYH11 and CNN1, and P27 (p27^{KIP1}), an antiproliferative cyclin-dependent kinase inhibitor, but reduced the pro-proliferative factor CCND1 (Cyclin D1) and the ECM protein collagen-1 (Figure 4B). These protein changes were accompanied by concordant transcriptional changes, including increased MYH11, CNN1, and CDKN1B (P27) mRNA levels and decreased expression of CCND1, CDK1, COL1A1, and COL3A1 (Figure 4C). Consistent with this phenotypic shift, BAHCC1 silencing inhibited SMC proliferation induced by either serum or PDGF-BB (Figure 4D), without detectable effects on apoptosis or cellular senescence (Figure S8). Furthermore, similar increases in MYH11, CNN1, and p27 protein levels were observed following BAHCC1 knockdown in TNFα-stimulated human SMCs (Figure S9), suggesting that the regulatory function of BAHCC1 in SMC phenotypic transition extends beyond PDGF-BB signaling. Importantly, in vivo immunofluorescence indicated that BAHCC1 knockdown elevated CNN1 and MYH11 in both the media and neointima while reducing proliferation as measured by PCNA expression (Figure 4E through 4G), linking BAHCC1's function in SMC phenotypic modulation in vitro and in vivo. Collectively, these data indicate that elevated BAHCC1 promotes pro-IH SMC phenotypic transition, revealing BAHCC1 as a novel modulator of SMC phenotype.

We next determined the mechanism underlying PDGF-stimulated BAHCC1 elevation in SMCs. Through the Genome Browser (http://genome.ucsc.edu/), nuclear transcription factor Y subunit alpha (NFYA) was predicted as a potential regulator of BAHCC1 expression. Motif analysis via JASPAR (https://jaspar.elixir.no/; Figure 4H) identified putative NFYA binding sites in the BAHCC1 promoter. Interestingly, previous research has shown that inactivation of NFYA inhibits SMC proliferation and IH[35], in line with the function of BAHCC1 observed herein. We therefore examined whether BAHCC1 expression is regulated by NFYA. ChIP-qPCR confirmed NFYA binding to the BAHCC1 promoter in HAoSMCs, which was enhanced by PDGF-BB stimulation (Figure 4I). Consistently, PDGF-BB stimulated the expression of both NFYA and BAHCC1, and silencing NFYA with shRNA (Figure S10) reduced BAHCC1 mRNA and prevented PDGF-BB induction of BAHCC1 protein (Figure 4J and 4K). Moreover, pharmacological inhibition of the PDGF-activated PI3K-Akt pathway using wortmannin or MK2206 led to decreased expression of both NFYA and BAHCC1 (Figure 4L). Collectively, these findings identify

Figure 1 Continued. control samples. Green: elastic laminae autofluorescence. Scale bar: 100 μm. Quantification: n=5 patients; Mann-Whitney *U* test. **D**, BAHCC1 (red) and αSMA (green) immunostaining in uninjured and injured rat carotid arteries. Note that BAHCC1 is predominantly localized to the nucleus, whereas αSMA is primarily cytoplasmic. Neointimal hyperplasia (IH) was induced by balloon angioplasty. Arteries were collected on postinjury days 3, 7, and 14. Scale bar: 100 μm. Quantification: n=4 rats; Kruskal-Wallis test with Benjamini-Krieger-Yekutieli post hoc correction (adjusted *P* values are shown on the graph). All data are presented as mean ± SEM. Arrowheads indicate the internal elastic lamina (IEL). A indicates adventitia; L, lumen; M, media; and N, neointima.

Downloaded from http://ahajournals.org by on November 5, 2026

Circulation Research FIRST PROOF ONLY

Downloaded from http://ahajournals.org by on November 5, 2026

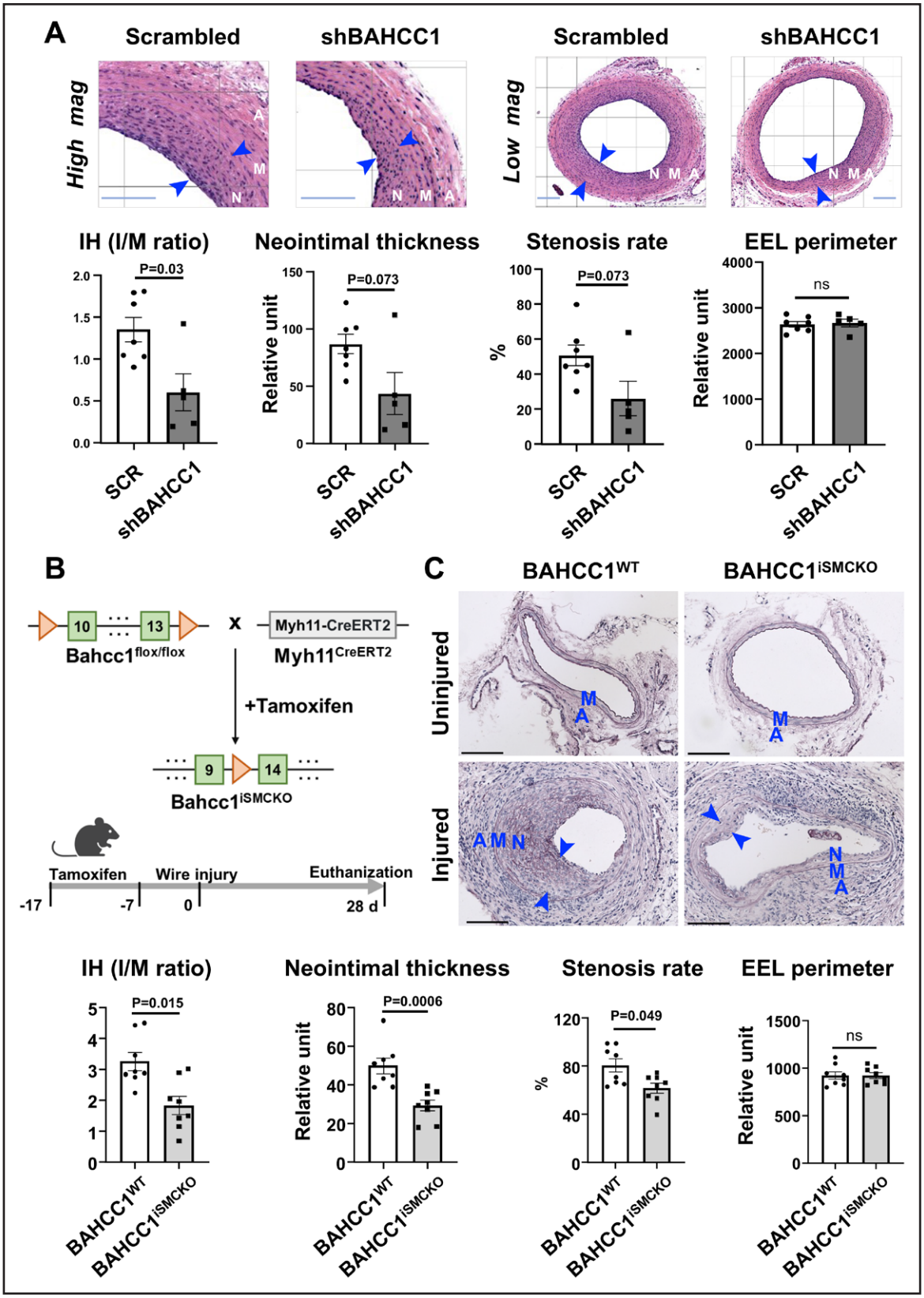


Figure 2. Loss of BAHCC1 (bromo adjacent homology domain coiled-coil 1) reduces neointimal hyperplasia (IH) in rat and mouse arteries.

A, **Top**: IH in balloon-injured Sprague-Dawley (SD) rat arteries. Injured arteries were infused with lentivirus to express scrambled or BAHCC1-specific shRNA and collected on postinjury day 14 for cross-sectioning and hematoxylin and eosin staining. Neointimal thickness is demarcated by arrowheads. **Bottom**: Quantitative analysis of the neointima/media area (I/M) ratio, neointimal thickness, stenosis rate, (*Continued*)

a previously unrecognized PI3K-Akt-NFYA-BAHCC1 signaling axis that mediates BAHCC1 upregulation in PDGF-activated SMCs (diagrammed in Figure 4M).

LMO7 Is a Direct Target of BAHCC1-H3K27me3–Mediated Gene Repression

To uncover downstream pathways through which BAHCC1 regulates SMC phenotypic transition, we performed bulk RNA sequencing and cleavage under targets and tagmentation (CUT&Tag) using HAoSMCs. Given the reported role of BAHCC1 in gene repression[21], we focused on genes that were upregulated upon BAHCC1 knockdown, assuming these were derepressed target genes. Among the top upregulated candidate genes ranked by *P* value and fold change (Figure 5A; Figure S11) and occupied by BAHCC1 (Figure S11D), LMO7 stood out for its reported role in modulating SMC phenotype and limiting IH[29]. We therefore prioritized LMO7 as a key downstream target for investigating the BAHCC1-directed epigenetic mechanisms that govern SMC phenotypic modulation.

We confirmed LMO7 upregulation at both mRNA and protein levels following BAHCC1 knockdown (Figure 5B and 5C). To determine whether BAHCC1 regulates LMO7 directly, potentially by recognizing H3K27me3 at the LMO7 locus, we performed ChIP-qPCR with HAoSMCs. Results showed that BAHCC1 physically associates with the LMO7 promoter and that this interaction is enhanced by PDGF-BB stimulation (Figure 5D).

To investigate whether this BAHCC1 association with the LMO7 gene depends on H3K27me3 recognition, we utilized aortic SMCs isolated from WT mice and mice bearing the Y2537A mutation, which disrupts BAHCC1's ability to bind H3K27me3. In WT mouse SMCs, PDGF-BB increased BAHCC1 binding at the LMO7 locus (Figure 5E), consistent with the observation in human SMCs (Figure 5D). Interestingly, H3K27me3 was also enriched at the LMO7 promoter in WT mouse SMCs, especially following PDGF-BB stimulation (Figure 5F). Reinforcing this observation, ChIP sequencing data from rat arteries revealed H3K27me3 enrichment at the LMO7 locus, with higher levels in injured arteries compared with uninjured controls (Figure 5G). Importantly, the binding of BAHCC1 at the LMO7 locus was markedly reduced in BAHCC1^{Y2537A} mouse SMCs compared with WT cells (Figure 5H), suggesting an important role of the BAHCC1-H3K27me3 dyad in regulating LMO7 expression. Indeed, LMO7 mRNA expression (Figure 5I) and protein production (Figure S12) were both increased (derepressed) in BAHCC1^{Y2537A} SMCs compared with WT SMCs.

To further establish the functional role of H3K27me3 in BAHCC1-mediated LMO7 repression, we used epigenetic editing. Instead of deleting the LMO7 promoter via genome editing—an approach that would interfere with transcription—we used a dCas9-EZH2 fusion system guided by LMO7-specific sgRNAs to enhance local H3K27me3 deposition (Figure 5J). ChIP-qPCR with cells overexpressing dCas9-EZH2 (Figure 5K) confirmed that H3K27me3 enrichment was enhanced at the LMO7 locus by each of the 3 LMO7-specific sgRNAs compared with the sgRNA control, the empty vector without expressing an sgRNA (Figure 5L). Consequently, LMO7 protein was reduced in the cells expressing these LMO7 sgRNAs compared with the empty vector control (Figure 5M). Importantly, this repression of LMO7 expression was abolished when BAHCC1 was silenced (Figure 5N), indicating that both BAHCC1 and H3K27me3 are required to repress LMO7 expression. Collectively, these findings demonstrate that the H3K27me3-reading/binding function of BAHCC1 plays a crucial role in its repression of LMO7 in SMCs.

LMO7 Silencing Reverses the Effects of BAHCC1 Loss on SMC Phenotype and IH

To determine the function of the BAHCC1-LMO7 axis in SMC phenotype and IH, we examined whether LMO7 knockdown could reverse the effects of BAHCC1 silencing. We first assessed markers of SMC differentiation (CNN1), inhibition of proliferation (P27), and extracellular matrix production (collagen-1; Figure 6A), as well as cell proliferation (Figure 6B), in vitro in HAoSMCs. Indeed, while BAHCC1 knockdown increased CNN1 and P27 expression, decreased collagen-1 levels, and inhibited proliferation, these effects were largely reversed by simultaneous LMO7 knockdown, highlighting its role downstream of BAHCC1.

To validate the BAHCC1-LMO7 axis in vivo, we determined LMO7 expression across 3 independent loss-of-function models. LMO7 was consistently upregulated following BAHCC1 silencing in injured

Figure 2 Continued. and EEL perimeter; n=7 or 5 rats; Mann-Whitney *U* test. **B**, **Top**: Strategy for generating the *Bahcc1*-floxed mouse line and tamoxifen-induced vascular smooth muscle cell (SMC)-specific BAHCC1 knockout with exons 10 to 13 deleted. **Bottom**: Experimental timeline. Mice received tamoxifen for 10 days. Wire injury was performed 7 days after tamoxifen was stopped. Animals were euthanized 28 days after surgery. **C**, **Top**: IH in wire-injured BAHCC1^{WT} and BAHCC1^{iSMCKO} arteries in male mice. Injured femoral arteries and uninjured contralateral arteries were collected on postinjury day 28 for cross-sectioning and Verhoeff-van Gieson staining. **Bottom**: Quantitative analysis of the I/M ratio, neointimal thickness, stenosis rate, and EEL perimeter; n=8 mice for each group; Mann-Whitney *U* test. BAHCC1^{WT}: tamoxifen-treated *Bahcc1*$^{fl/fl}$ mice. BAHCC1^{iSMCKO}: tamoxifen-treated *Bahcc1*$^{fl/fl}$*; Myh11-CreER*^{T2}*-RAD* mice. The cartoon on the left illustrates wire injury of the femoral artery to induce IH. All data are presented as mean ± SEM; Scale bar: 100 μm. A indicates adventitia; M, media; N, neointima; and ns, not significance.

Downloaded from http://ahajournals.org by on November 5, 2026

Circulation Research FIRST PROOF ONLY

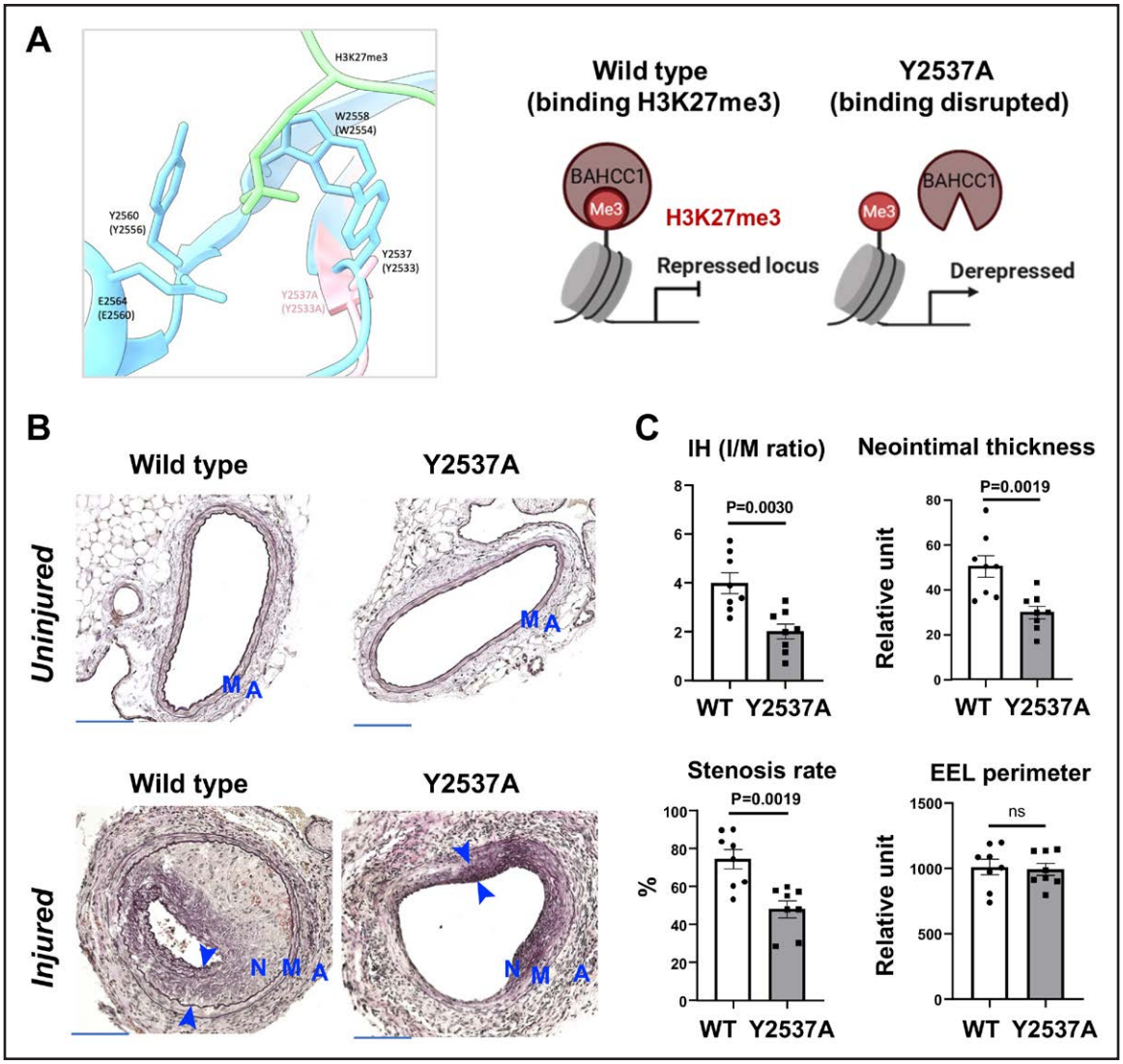


Figure 3. Disruption of BAHCC1 (bromo adjacent homology domain coiled-coil 1)-histone-3 lysine 27 trimethylation (H3K27me3) binding reduces neointimal hyperplasia (IH) in mouse arteries.
A, **Left**: Modeling of BAHCC1^{BAH}-H3K27me3 binding. The crystal structure of BAHCC1^{BAH} (PDB 6VIL) is shown in blue, and the AlphaFold3-predicted Y2537A mutant model is shown in salmon. The H3K27me3 peptide from the crystal structure is green. The wild-type (WT) BAHCC1^{BAH} was aligned with the Y2537A model for comparison. In the WT structure, residues Y2537, W2558, Y2560, and E2564 surround the H3K27me3 peptide from multiple directions, forming a pocket that stabilizes the interaction. In the Y2537A model, substitution of Tyr with Ala alters this pocket, leaving 1 side open. This structural change is predicted to compromise BAHCC1^{BAH}-H3K27me3 binding. The equivalent amino acids in the human BAHCC1^{BAH} sequence are presented in parentheses. **Right**: Cartoon presentation depicting how the BAHCC1^{Y2537A} mutation disrupts the interaction between BAHCC1^{BAH} and H3K27me3. **B**, IH in wire-injured WT and BAHCC1^{Y2537A} homozygous male mouse arteries. Injured femoral arteries and uninjured contralateral arteries were collected on postinjury day 28 for cross-sectioning and Verhoeff-van Gieson staining. Neointima is demarcated by arrowheads. **C**, Quantitative analysis of the neointima/media area (I/M) ratio, neointimal thickness, stenosis rate, and EEL perimeter. n=8 mice for each group; Mann-Whitney *U* test. All data are presented as mean ± SEM; Scale bar: 100 μm. A indicates adventitia; M, media; N, neointima; and ns, not significance.

rat arteries (Figure 6C), genetic ablation of BAHCC1 in SMCs (Figure 6D), and disruption of BAHCC1's H3K27me3-reader function in BAHCC1^{Y2537A} mice (Figure 5I and Figure S12). The concordance of these independent models provides strong evidence that BAHCC1 represses LMO7 expression in vivo through its H3K27me3-reader activity.

Given the IH-mitigating effect of BAHCC1^{Y2537A} observed herein and the reported IH-inhibitory role of LMO7[29], we inferred that silencing LMO7 in BAHCC1^{Y2537A} mouse arteries would reverse the effect of this mutation on IH. Indeed, lentiviral shRNA-mediated knockdown of LMO7 (Figure S13) significantly increased IH in injured femoral arteries of BAHCC1^{Y2537A} mice compared with scrambled controls (Figure 6E). There were no significant changes in EEL perimeter. These results establish the BAHCC1-LMO7 axis as a key determinant of SMC phenotypic transition and IH progression.

Downloaded from http://ahajournals.org by on November 5, 2026

Downloaded from http://ahajournals.org by on November 5, 2026

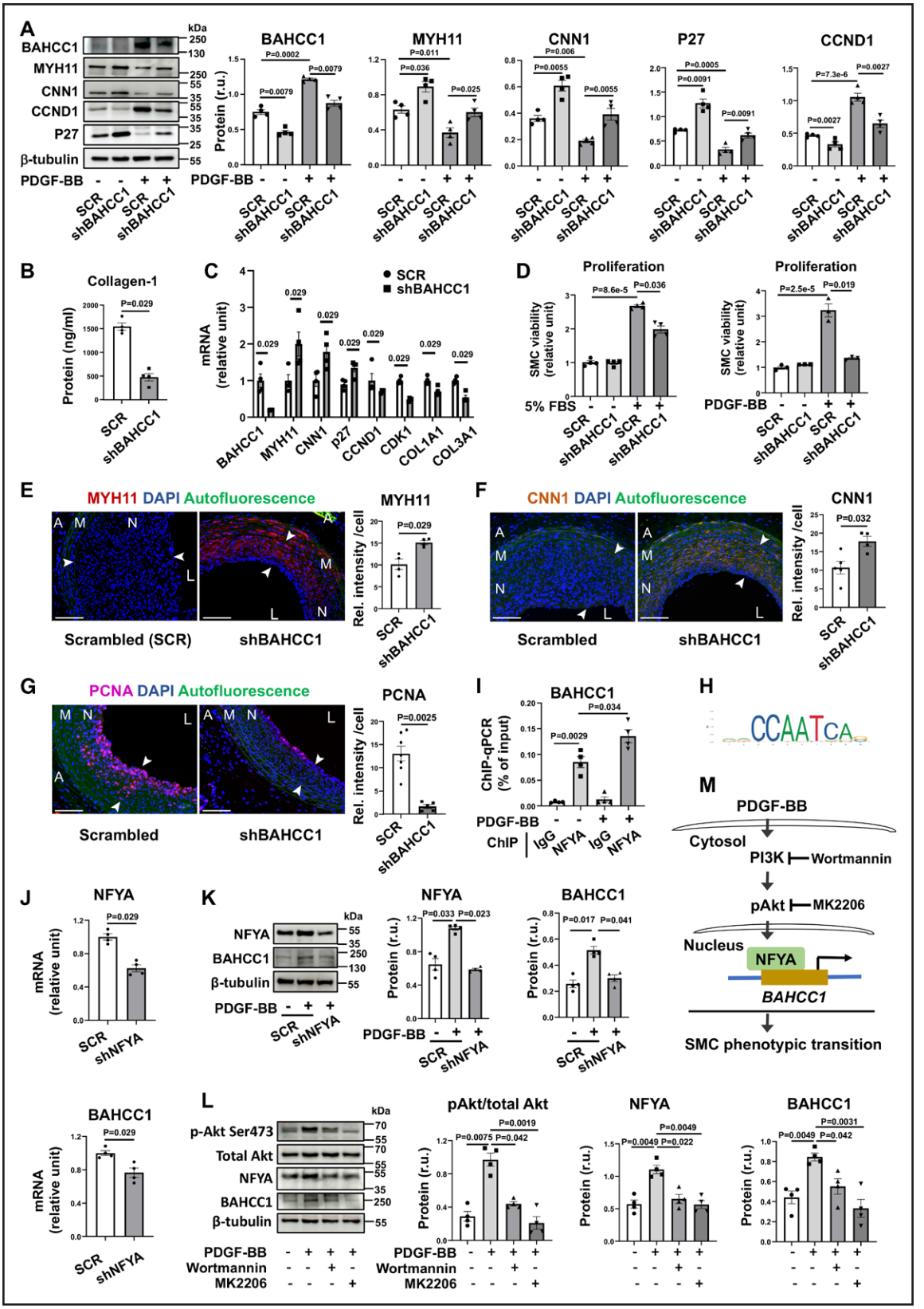


Figure 4. BAHCC1 (bromo adjacent homology domain coiled-coil 1) promotes vascular smooth muscle cell (SMC) phenotypic transition and is regulated by NFYA (nuclear transcription factor Y subunit alpha).

A, Western blots of BAHCC1, MYH11, CNN1, CCND1 (cyclin D1), and p27 in human aortic SMCs (HAoSMCs) infected with lentivirus (LV)-shRNA-scramble (SCR) or shRNA-BAHCC1 with or without PDGF-BB stimulation. Quantification: n=4 independent repeat experiments; 2-way aligned rank transform (ART) ANOVA with Holm post hoc test (adjusted *P* values are shown on the graph). BAHCC1 (*Continued*)

BAHCC1 Forms a Repressive Complex With SAP30-RBBP4/7 to Regulate LMO7 Expression and SMC Phenotypic Transition

To further dissect the mechanism of BAHCC1-mediated gene regulation, we sought to identify corepressors that cooperate with BAHCC1. Protein interaction predictions using STRING[36] suggested that SAP30 (SIN3-associated protein 30), RBBP4 (retinoblastoma-binding protein 4), and RBBP7 (retinoblastoma-binding protein 7) may interact with BAHCC1. Immunoprecipitation of any of these individual proteins (BAHCC1, SAP30, RBBP4, or RBBP7) could co-IP each of the others in HEK293T cells (Figure 7A), suggesting formation of a stable complex. Proximity ligation assay signals in the nuclei further confirmed BAHCC1 interaction with each of the 3 proteins in HAoSMCs, which was enhanced by PDGF-BB stimulation (Figure 7B).

To explore the potential structural basis for this complex, we performed molecular modeling with the AlphaFold3 server[37] using the sequences in UniProt[38] that correspond to existing 3D structural data for BAHCC1^{BAH}, tandem Tudor domains (BAHCC1^{TTD}), SAP30, RBBP4, and RBBP7. The model in Figure 7C represents the highest-ranking prediction generated via AlphaFold3, in which SAP30 appears to play a central role in the complex by mediating interactions with BAHCC1. Specifically, SAP30 residues 16 to 27 and 56 to 63 contact BAHCC1^{BAH} residues 2542 to 2548, 2556 to 2560, and 2584 to 2588, whereas SAP30 residues 169 to 173 are placed adjacent to BAHCC1^{TTD} residues 1920 to 1926 within the first Tudor domain; overall, BAHCC1^{BAH} is predicted to contribute more favorably to the complex formation than TTD.

As gene-repressive roles of RBBP4/7 and SAP30 have been reported[39], we hypothesized that BAHCC1, RBBP7, RBBP4, and SAP30 form a repressive complex at the target gene LMO7. We thus performed CUT&Tag in HAoSMCs using antibodies against these 4 proteins. Genomic analysis showed similar enrichment patterns around the transcription start site (Figure 7D). Genomic occupancy by these proteins was detected essentially across all chromosomes (Figure 7E), and peaks were predominantly located in intergenic, intronic, and promoter regions (Figure 7F). Of note, CUT&Tag revealed cooccupancy of all 4 proteins near the LMO7 transcription start site (Figure 7G). This was further confirmed by ChIP-qPCR showing that RBBP7, RBBP4, and SAP30 were enriched at the same site, and that their enrichment was reduced following BAHCC1 knockdown (Figure 7H). Consistent with a cooperative role in gene repression, silencing of RBBP7, RBBP4, and SAP30 (Figure S14) led to increased LMO7 expression (Figure S15). These data demonstrate that BAHCC1 and its corepressors RBBP7, RBBP4, and SAP30 form a functional complex to repress LMO7's expression.

We then determined the role of this gene-repression complex in SMC phenotypic modulation. As shown in Figure 7I, silencing RBBP7, RBBP4, or SAP30 reduced SMC proliferation, closely resembling the effect of BAHCC1 knockdown (Figure 4D). In accordance, CUT&Tag showed coenrichment of BAHCC1 with these corepressors at the antiproliferative gene P27 (Figure 7J). Furthermore, while PDGF-BB promoted BAHCC1 binding at P27 (Figure 7K) and contractile SMC phenotype genes (CNN1, MYH11; Figure S16), the binding of its corepressors at these loci was attenuated by BAHCC1 silencing (Figure S16).

Together, these findings demonstrate that BAHCC1 functions in a complex with SAP30, RBBP4, and RBBP7 to drive pro-IH SMC plasticity by repressing LMO7 and potentially other genes involved in SMC phenotype (Figure S17).

Genetic Variation of BAHCC1 Is Associated With Cardiovascular Phenotypes

Accumulating evidence indicates that SMC plasticity is a central mechanism underlying vascular remodeling

Downloaded from http://ahajournals.org by on November 5, 2026

Circulation Research FIRST PROOF ONLY

Figure 4 Continued. corresponds to the β-tubulin blot shown here, and each target protein was quantified using its own loading control. **B**, ELISA of collagen-1 in the culture medium of HAoSMCs infected with LV-shRNA-SCR or LV-shRNA-BAHCC1. Quantification: n=4 independent repeat experiments; Mann-Whitney *U* test. **C**, RT-qPCR of relative mRNA levels of BAHCC1, CNN1, MYH11, P27, CCND1, CDK1, COL1A1, and COL3A1 in HAoSMCs infected with LV-shRNA-SCR or LV-shRNA-BAHCC1. Quantification: n=4 independent repeat experiments, Mann-Whitney *U* test. **D**, Proliferation of human and rat SMCs infected with LV-shRNA-SCR or LV-shRNA-BAHCC1 and treated with or without FBS or PDGF-BB. Quantification: n=4 or 3 independent repeat experiments; 2-way ART ANOVA with Holm post hoc test (adjusted *P* values are shown on the graph). **E** through **G**, Immunostaining of MYH11 (red), CNN1 (orange), and PCNA (magenta) in injured rat arteries treated with LV-shRNA-SCR or LV-shRNA-BAHCC1 and collected on postinjury day 14. Neointimal thickness is demarcated by arrowheads. Green: elastic laminae autofluorescence. Scale bar: 100 μm. Quantification: n=4 rats per group in **E**; n=5 or 4 rats in **F**; n=7 or 5 rats in G; Mann-Whitney *U* test. H. Sequence logo of NFYA. I. Binding of NFYA to the BAHCC1 promoter in HAoSMCs assessed by ChIP-qPCR. Quantification: n=4 independent repeat experiments; 2-way ART ANOVA with Holm post hoc test (adjusted *P* values are shown on the graph). **J**, RT-qPCR of relative mRNA levels of NFYA and BAHCC1 in HAoSMCs infected with LV-shRNA-SCR or LV-shRNA-NFYA. Quantification: Mann-Whitney *U* test; n=4 independent repeat experiments. **K**, Western blots of NFYA and BAHCC1 in HAoSMCs infected with LV-shRNA-SCR or LV-shRNA-NFYA, with or without PDGF-BB stimulation. Quantification: n=4 independent repeat experiments; Kruskal-Wallis test with Benjamini-Krieger-Yekutieli post hoc correction (adjusted *P* values are shown on the graph). **L**, Western blots of pAkt, NFYA, and BAHCC1 in HAoSMCs treated with wortmannin or MK2206, with or without PDGF-BB stimulation. Quantification: n=4 independent repeat experiments; Kruskal-Wallis test with Benjamini-Krieger-Yekutieli post hoc correction (adjusted *P* values are shown on the graph). **M**, Schematic of the pathway by which PDGF-BB stimulates BAHCC1 expression via PI3K-Akt-NFYA. All data are presented as mean ± SEM. A indicates adventitia; L, lumen; M, media; and N, neointima.

Downloaded from http://ahajournals.org by on November 5, 2026

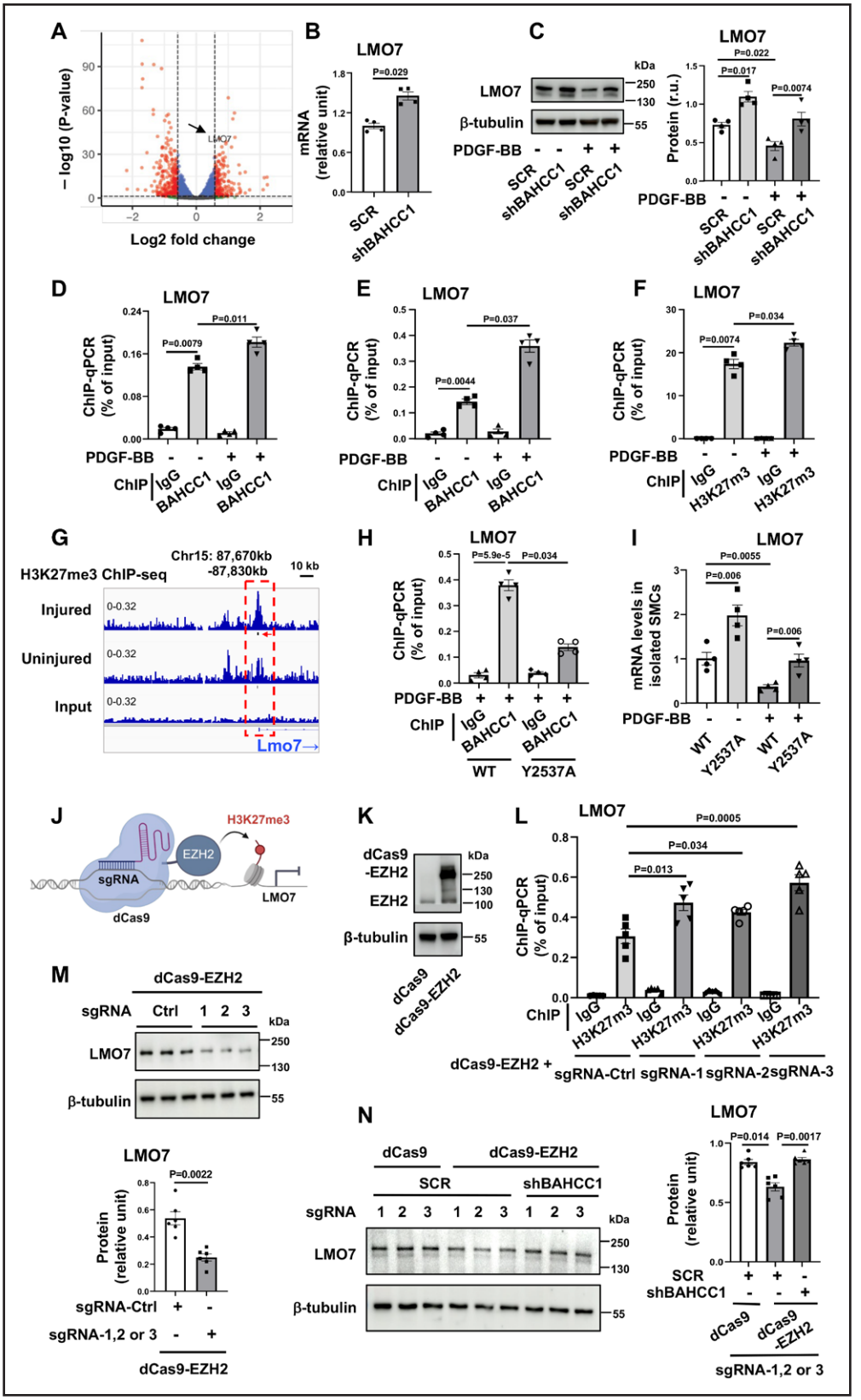


Figure 5. The BAHCC1 (bromo adjacent homology domain coiled-coil 1)-histone-3 lysine 27 trimethylation (H3K27me3) dyad regulates LMO7 (LIM domain only 7) expression.

A, Volcano plot. A total of 13 694 variables are included. Adjusted *P* values are presented. Fold change: shBAHCC1 vs scrambled (SCR). HAoSMCs were infected with LV-shRNA-SCR or LV-shRNA-BAHCC1. N=3 separate HAoSMC cultures. **B** and **C**, RT-qPCR and Western blots of LMO7 expression in HAoSMCs infected with LV-shRNA-SCR or LV-shRNA-BAHCC1, with or without PDGF-BB stimulation. (*Continued*)

across multiple cardiovascular pathologies, including atherosclerosis, restenosis, and hypertension[34]. We thus investigated the potential relevance of BAHCC1 to human cardiovascular disease (CVD). We queried the locus containing BAHCC1 using publicly available genome-wide association study data sets for cardiovascular phenotypes and identified several genome-wide significant variants (Figure 8A). In particular, rs6565564 showed strong associations with CVD (P=1×10^{-08})[40] and hypertension (P=2×10^{-10})[41]. Linkage disequilibrium analysis revealed that a group of upstream variants display high linkage disequilibrium (r^2>0.8) with rs6565564 (Figure 8B, arrow), and this region showed BAHCC1 enrichment based on the CUT&Tag data (Figure 8B). Analysis of the Genotype-Tissue Expression database showed that rs6565564 is an expression quantitative trait locus in arterial tissues (Figure 8C), with the minor allele associated with increased BAHCC1 expression relative to the reference allele (normalized effect size=0.29; Figure S18). Further supporting a link between BAHCC1 genetic variation and CVD, rs4969440, a variant identified in the Million Veteran Program meta-analysis, showed a suggestive association (P=1.8×10^{-06}) with atherosclerosis (PheCode 440)[42]. Together, these integrated genomic and epigenomic findings provide strong evidence that BAHCC1 variation influences arterial gene regulation and is associated with cardiovascular traits, implicating BAHCC1 dysregulation as a potential contributor to human vascular pathology.

DISCUSSION

The dedifferentiation of vascular SMCs underlies both adaptive vascular remodeling and IH, a complication of revascularizations including angioplasty, stenting, bypass grafting, endarterectomy, and arteriovenous fistula creation[2]. Increasing evidence supports the concept that reversible epigenetic marks likely underlie this plasticity. While research has focused on the writers and erasers of these marks, such as DNMTs and TET2[14, 43], or p300 and HDACs[16, 17], few studies have addressed the roles of epigenetic readers, proteins that bind these modifications to mediate activation or repression of gene transcription. Our laboratory previously revealed a key role for BRD4[27], a reader of activating histone acetylation marks. We now demonstrate a critical role for BAHCC1, a reader of the repressive mark H3K27me3, in promoting SMC dedifferentiation, proliferation, and IH.

Our study uncovers novel insights into histone methylation-mediated gene repression in IH pathogenesis—a particularly underexplored area[19, 44-48]. We demonstrate: (1) BAHCC1 is upregulated in human and rat IH lesions and promotes IH by negating the IH suppressor LMO7; (2) this pro-IH function of BAHCC1 is dependent on its ability to read H3K27me3; (3) BAHCC1 forms a complex with SAP30 and RBBP4/7 to repress gene expression, facilitating pro-IH SMC phenotypic transition; and (4) upregulation of BAHCC1 in human SMCs is driven by transcription factor NFYA. In addition, analysis of public data sets links BAHCC1 genetic variation with human cardiovascular phenotypes and increased BAHCC1 expression. In summary, this study identifies the gene-repression epigenetic reader BAHCC1 as a previously unrecognized regulator of SMC phenotypic plasticity and IH pathophysiology and reveals its regulatory mechanisms.

BAHCC1's biological functions remain underexplored, despite prior progress linking it to cancer progression and metastasis[20-22, 49], neuronal commitment[31, 50], and proinflammatory gene expression[51]. To our knowledge, the current study is the first to identify BAHCC1's role in vascular disease, specifically through its H3K27me3-reader function. This expands upon our previous finding that inhibition of H3K27me3 deposition attenuates IH in rats[23, 52]. In accordance, BAHCC1 silencing mitigated IH in the same model of

Circulation Research FIRST PROOF ONLY

Downloaded from http://ahajournals.org by on November 5, 2026

Figure 5 Continued. Quantification for **B**: Mann-Whitney *U* test; n=4 independent repeat experiments. Quantification for **C**: 2-way aligned rank transform (ART) ANOVA with Holm post hoc test (adjusted *P* values are shown on the graph); n=4 independent repeat experiments. **D**, Binding of BAHCC1 at the LMO7 promoter in HAoSMCs assessed by ChIP-qPCR. Quantification: n=4 independent repeat experiments; 2-way ART ANOVA with Holm post hoc test (adjusted *P* values are shown on the graph). **E** and **F**, Binding of BAHCC1 and H3K27me3 at the LMO7 promoter in mouse aortic vascular smooth muscle cells (SMCs), assessed by ChIP-qPCR. Quantification (**E** and **F**): n=4 independent repeat experiments; 2-way ART ANOVA with Holm post hoc test (adjusted *P* values are shown on the graph). **G**, IGV plots showing H3k27me3 peaks at the LMO7 gene locus (boxed). ChIP-seq was performed using sham (uninjured) and injured rat carotid artery tissues. The red arrow points to a super-silencer region. **H**, Binding of BAHCC1 at the LMO7 promoter in wild-type (WT) and BAHCC1^{Y2537A} mouse aortic SMCs, assessed by ChIP-qPCR. Quantification: n=4 independent repeat experiments; 2-way ART ANOVA with Holm post hoc test (adjusted *P* values are shown on the graph). **I**, RT-qPCR analysis of the relative mRNA levels of LMO7 in WT and BAHCC1^{Y2537A} mouse aortic SMCs. Quantification: 2-way ART ANOVA with Holm post hoc test (adjusted *P* values are shown on the graph); n=4 independent repeat experiments. **J**, Schematic of locus-specific epigenetic editing. The dCas9-EZH2 fusion protein is expressed and directed by an sgRNA to the LMO7 locus, where H3K27me3 is increased, resulting in repression of LMO7 gene expression. **K**, Western blot of dCas9-EZH2 fusion protein expression in 293T cells. **L**, H3K27me3 enrichment levels at the LMO7 promoter in 293T cells transfected with dCas9-EZH2 plus each of 3 sgRNA-LMO7 constructs, compared with dCas9-EZH2 plus sgRNA control (empty vector), assessed by ChIP-qPCR. Quantification: Kruskal-Wallis test with Benjamini-Krieger-Yekutieli post hoc correction (adjusted *P* values are shown on the graph); n=5 independent repeat experiments. **M**, Western blots showing LMO7 levels in 293T cells transfected with the dCas9-EZH2 vector together with sgRNA control or each of 3 LMO7 sgRNAs. Quantification: Mann-Whitney *U* test; n=6 independent repeat experiments. **N**, Western blots indicating the effect of BAHCC1 silencing on dCas9-EZH2-mediated repression of LMO7 expression. Quantification: Kruskal-Wallis test with Benjamini-Krieger-Yekutieli post hoc correction (adjusted *P* values are shown on the graph); n=6 independent repeat experiments. All data are presented as mean ± SEM.

Downloaded from http://ahajournals.org by on November 5, 2026

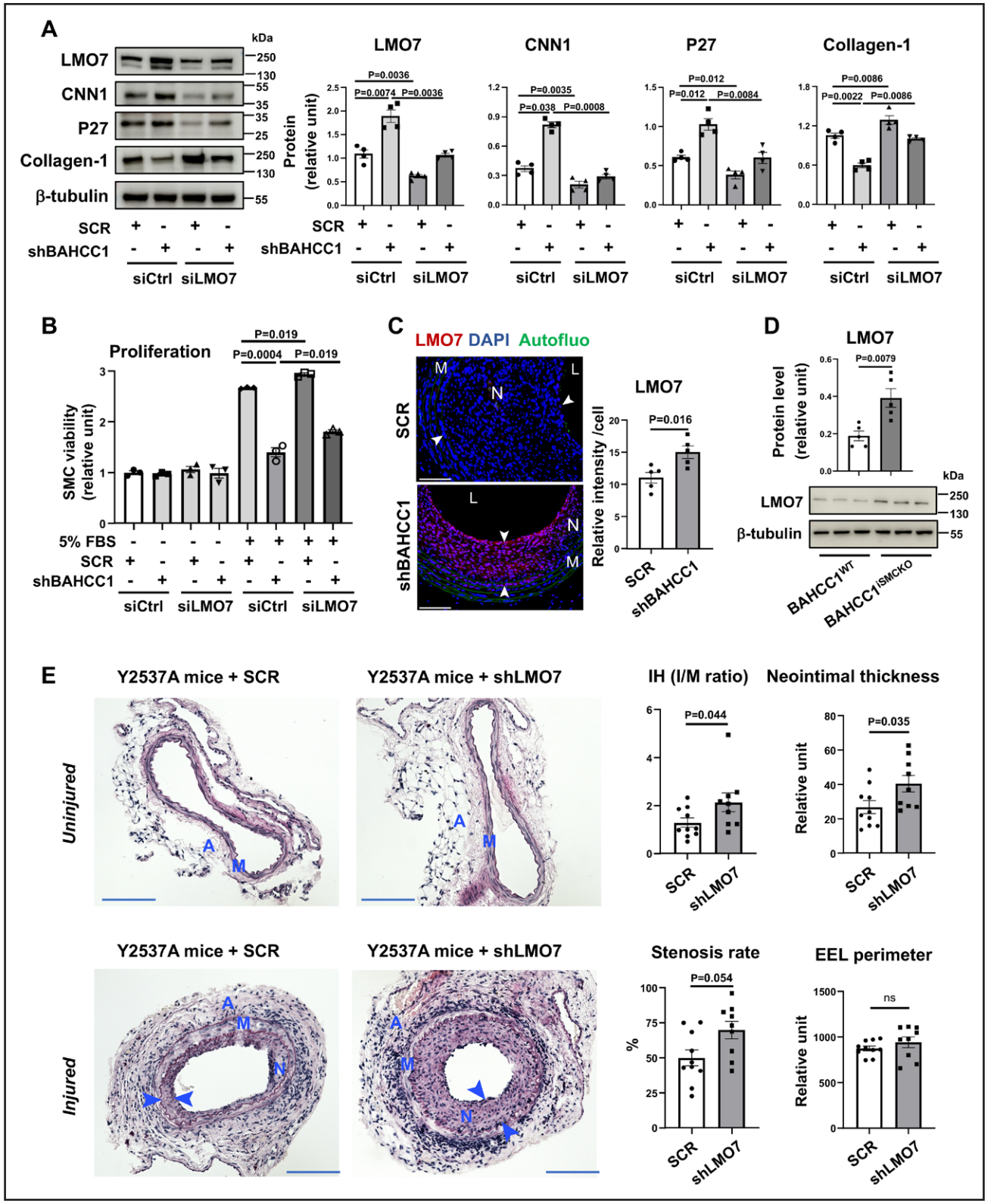


Figure 6. The BAHCC1 (bromo adjacent homology domain coiled-coil 1)-LMO7 (LIM domain only 7) axis in the regulation of neointimal hyperplasia (IH).

A, Western blot of LMO7, CNN1, P27, and collagen-1 in HAoSMCs infected with LV-shRNA-SCR or LV-shRNA-BAHCC1 and transfected with siRNA-Ctrl or siRNA-LMO7. Quantification:2-way aligned rank transform (ART) ANOVA with Holm post hoc test (adjusted *P* values are shown on the graph); n=4 independent repeat experiments. CNN1 corresponds to the beta-tubulin blot shown here, and each target protein was quantified using its own loading control. **B**, Proliferation of HAoSMCs infected with LV-shRNA-SCR or LV-shRNA-BAHCC1 and transfected with siRNA-Ctrl or siRNA-LMO7, with or without FBS stimulation. Quantification: 2-way ART ANOVA with Holm post hoc test (*Continued*)

rat carotid artery injury, and SMC-specific BAHCC1 depletion in injured mouse arteries had a similar effect. BAHCC1 is a multidomain large protein with at least 2 reader modules[21, 30], and an H3K27me3-independent, pro-proliferative function has been reported in melanoma cells[22]. In contrast, we identified the critical role of BAHCC1-H3K27me3 in IH using mice with the Y2537A knock-in mutation in the H3K27me3-reading BAH domain, which directly and specifically disrupts this reader-mark dyad.

Through epigenomic and transcriptomic analyses, together with in vitro and in vivo validations, we have further unraveled the underlying molecular mechanism by demonstrating that BAHCC1-H3K27me3 orchestrates the epigenetic repression of LMO7, a regulator of SMC phenotype and suppressor of IH, as reported previously[29] and documented herein. Given the limited attention to H3K27me3-mediated gene-repression mechanisms in IH research, our study sheds new light on epigenetic regulations of vascular diseases. Importantly, our findings also reveal BAHCC1-LMO7 as a novel axis in IH pathobiology. Silencing BAHCC1 increases LMO7 expression while attenuating the pro-IH SMC phenotypic transition characterized by changes in SMC markers, proliferation, and collagen production. Rescue experiments of silencing LMO7 in the BAHCC1-silenced background, on the other hand, reverse this effect. Moreover, silencing LMO7 in BAHCC1-inactivated BAHCC1^{Y2537A} mouse arteries counteracted the IH-mitigating effect of this mutation. Thus, we have identified a repression-of-suppressor mechanism in IH pathophysiology mediated by the BAHCC1-H3K27me3 epigenetic dyad.

We have established LMO7 as a direct BAHCC1 target through multiple methods, including epigenetic editing of H3K27me3 enrichment at the *LMO7* locus. Together with the prior published functions of LMO7 in SMCs as a negative feedback regulator of profibrotic signaling that limits IH[29], our rescue experiments suggest that BAHCC1 regulation of LMO7 exerts a powerful role in SMC phenotypic switching in vascular remodeling. It is likely that other BAHCC1 targets also contribute to the dramatic protective phenotype seen with SMC-specific BAHCC1 knockout. Indeed, CUT&Tag epigenomic profiling revealed that BAHCC1 and its corepressors target additional genes key to SMC phenotype, including the antiproliferative genes P27 and P15, as well as the SMC contractile gene SM22 (Figure S19). These data support a model in which BAHCC1 governs SMC phenotype by repressing LMO7, which in turn regulates downstream genes, and also by directly occupying antiproliferative and contractile loci (eg, P27, P15, SM22, CNN1) to limit their expression. Of note, further illustrating the breadth of BAHCC1-directed gene repression related to IH, CUT&Tag analysis also revealed enrichment of BAHCC1/corepressors at another IH suppressor (Figure S20), REST (RE1-silencing transcription factor)[53], although it was less prominent than LMO7 in our RNA sequencing data set. Together, these findings underscore BAHCC1 as a master regulator of SMC plasticity, likely by orchestrating epigenetic repression of multiple pathways.

Previous work indicated ING1/2, HDAC1, and SAP30BP as BAHCC1's corepressors in a cancer cell line[21]. Our data instead reveal that, in human SMCs, BAHCC1 forms a novel complex with SAP30 and RBBP4/7. Silencing components of this complex upregulates LMO7 expression, consistent with the established gene-repressive functions of SAP30 and RBBP4/7[39]. RBBP4/7 are shared core components of several chromatin-associated complexes, including the SIN3 family and PRC2, whereas SAP30 is specific to SIN3 complexes and absent from PRC2[20,54]. Our findings therefore point to a previously unrecognized SIN3 complex featuring BAHCC1-SAP30-RBBP4/7 that regulates SMC pathobiology. While this article was in preparation, another group reported a co-IP-based BAHCC1 association with SIN3A, a scaffold protein in SIN3 complexes, in a neuronal cell line[31]. However, they observed notable functional differences: BAHCC1's function appeared to be H3K27me3-independent and it functioned as a gene activator rather than a repressor. These differences suggest that BAHCC1 may participate in distinct regulatory mechanisms depending on cellular and biological context, consistent with the compositional diversity of SIN3 complexes, which incorporate a variety of auxiliary factors beyond core components such as SAP30[31, 54]. Interestingly, AlphaFold3 structural modeling illustrates that both BAHCC1^{BAH} and BAHCC1^{TTD} can engage SAP30. In addition, although biochemical evidence supports the presence of SAP30 and RBBP4/7 within the same

Downloaded from http://ahajournals.org by on November 5, 2026

Circulation Research FIRST PROOF ONLY

Figure 6 Continued. (adjusted *P* values are shown on the graph); n=3 independent repeat experiments. **C**, Immunofluorescence of LMO7 (red) in balloon-injured rat carotid arteries infected with LV-shRNA-SCR or LV-shRNA-BAHCC1 on day 14 postsurgery. Scale bar = 100 µm. Neointimal thickness is demarcated by arrowheads. Quantification: n=5 rats per group; Mann-Whitney *U* test. **D**, Western blots indicating the effect of vascular smooth muscle cell (SMC)-specific BAHCC1 deletion on LMO7 expression. Aortic SMCs were isolated from BAHCC1^{WT} and BAHCC1^{iSMCKO} mice, cultured and starved, and then treated with PDGF-BB before cell harvest. Quantification: Mann-Whitney *U* test; n=5 independent repeat experiments. **E**, **Left**: Representative cross-sections of Verhoeff-van Gieson-stained wire-injured femoral arteries of BAHCC1^{Y2537A} male mice infected with LV-shRNA-SCR or LV-shRNA-LMO7. Arteries were collected 28 days after surgery. Scale bar: 100 µm. **Right**: Quantitative analysis of the corresponding injured arteries for the neointima/media area (I/M) ratio, neointimal thickness, stenosis rate, and EEL perimeter. Quantification: Mann-Whitney *U* test; n=10 or 9 mice for each group. All data are presented as mean ± SEM. A indicates adventitia; L, lumen; M, media; N, neointima; and ns, not significance.

ORIGINAL RESEARCH

Downloaded from http://ahajournals.org by on November 5, 2026

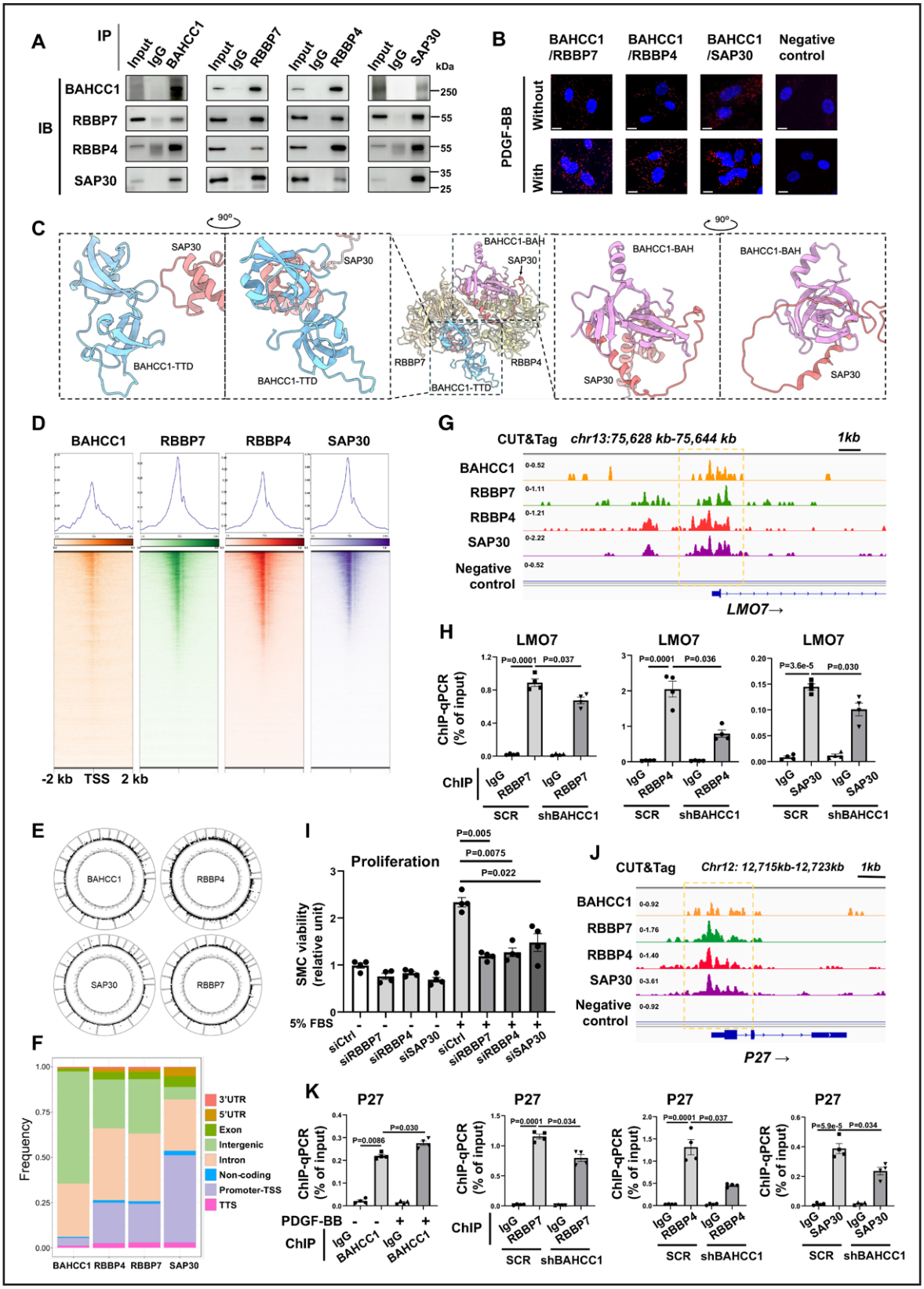


Figure 7. Cooperation of BAHCC1 (bromo adjacent homology domain coiled-coil 1), RBBP4/7, and SAP30 in regulating LMO7 (LIM domain only 7) expression and vascular smooth muscle cell (SMC) phenotypic transition.

A,Co-IP of BAHCC1, RBBP7, RBBP4, and SAP30 with each other in 293T cells. **B**, Proximity ligation assay (PLA) showing BAHCC1 interaction with each of the RBBP7, RBBP4, and SAP30 proteins in HAoSMCs, with or without PDGF-BB stimulation. Scale bar: 10 μm. A negative control assay was performed without a primary antibody. **C**, AlphaFold3 modeling of interactions between BAHCC1, RBBP7, RBBP4, (*Continued*)

SIN3 complex[55], a structure showing direct SAP30 interaction with RBBP4/7, as predicted here (Figure 7C), has not been reported. Together, our biochemical studies and AlphaFold3 prediction support a model in which BAHCC1 recruits SAP30 and RBBP4/7 to form a functional corepressor assembly. Further investigation of this BAHCC1-SAP30-RBBP4/7 regulatory machinery may uncover new epigenetic mechanisms governing SMC plasticity and IH pathophysiology.

A super-silencer refers to a cluster of H3K27me3-rich genomic regions that together facilitate gene repression and can be identified via algorithms based on H3K27me3 ChIP sequencing peaks[56]. Interestingly, a super-silencer was identified in the LMO7 promoter in injured rat artery tissues (Figure 5G). It is thus plausible to propose that the BAHCC1-H3K27me3 dyad and cofactors SAP30 and RBBP4/7, possibly together with a super-silencer(s), may constitute a context-dependent, LMO7-repressing silenceosome[57], 1 that may present a molecular vulnerability for effective therapeutic targeting to treat IH. While much attention has been given to enhancers in studies of epigenetics, silencers and associated complexes remain underexplored[56]. Future investigation into this silenceosome hypothesis is warranted.

While BAHCC1 expression is correlated with human cancers[22, 49, 58], our analysis of public genetic data sets reveals its relevance to human CVD for the first time. We identified a BAHCC1 variant (rs6565564) strongly associated with CVD[40] and hypertension[41], with the variant allele linked to increased BAHCC1 expression, and some polymorphisms as splicing quantitative trait loci (Figure S21). This aligns with our observations of BAHCC1 upregulation in human restenotic and atherosclerotic arteries and with RNA sequencing data showing enrichment of CVD pathways in response to BAHCC1 knockdown in human SMCs (Figure S11C). These findings underscore BAHCC1 as a clinically relevant player in vascular pathology and a potential therapeutic target. Despite its emerging importance, the mechanisms driving BAHCC1 upregulation remain poorly understood[22, 49]. Our identification of NFYA as a novel upstream regulator of BAHCC1 provides new avenues for translational development, including potential therapeutic strategies targeting the PI3K-Akt-NFYA-BAHCC1 pathway.

Study Limitations

Although our studies provide compelling evidence for BAHCC1's role in pro-IH SMC phenotypic transition, future research should investigate its cell type-specific functions via conditional knockout in fibroblasts and macrophages to offer a more comprehensive understanding of IH pathogenesis. While our focus was on BAHCC1's nuclear role, potential contributions of non-nuclear BAHCC1 to vascular dysregulation remain unexplored. In addition, future studies with larger cohorts will be helpful for defining potential sex-dependent differences in greater detail. Finally, developing therapeutic agents that selectively disrupt the BAHCC1-H3K27me3 dyad represents a promising step toward translating these findings into effective IH treatments.

Conclusions

Through transcriptomic and epigenomic analyses, epigenetic editing, conditional knockout, and rodent models, we identify BAHCC1 as a previously unrecognized epigenetic driver of IH. Mechanistically, BAHCC1 represses the IH-suppressor LMO7 and downstream genes via its H3K27me3-reader function, inducing SMC phenotypic transition and promoting IH. This mechanism entails a BAHCC1-corepressor complex formed with SAP30 and RBBP4/7, which could be further explored as a potential therapeutic target to address IH and related vascular pathologies.

Downloaded from http://ahajournals.org by on November 5, 2026

Circulation Research FIRST PROOF ONLY

Figure 7 Continued. and SAP30. The model was generated using the AlphaFold3 server with full-length human RBBP4, RBBP7, and SAP30, together with 2 fragments of BAHCC1: amino acids (aa) 1905 to 2037, corresponding to BAHCC1^{TTD}, and aa 2513 to 2639, corresponding to BAHCC1^{BAH}. Cartoon representations of protein structures are displayed. The central panel shows the overall structure and interactions within a multiprotein assembly containing BAHCC1^{BAH} (purple), BAHCC1^{TTD} (blue), SAP30 (salmon), RBBP7 (beige), and RBBP4 (yellow). The left panels depict the detailed interactions between BAHCC1^{TTD} and SAP30. Left panel 2 shows a zoomed-in view of the dashed box highlighted in the central panel. Left panel 1 presents orthogonal views of the interacting domains, rotated by 90°, to illustrate their 3-dimensional arrangement and binding interface. Likewise, the right panels depict the detailed interaction between BAHCC1BAH and SAP30. Right panel 1 shows a zoomed-in view of the dashed box highlighted in the central panel, while right panel 2 displays orthogonal views rotated by 90° to illustrate the binding interface. **D**, CUT&Tag heatmaps of BAHCC1, RBBP7, RBBP4, and SAP30 in HAoSMCs. One of 2 independent repeat experiments is shown. **E**, Genome coverage maps of BAHCC1, RBBP7, RBBP4, and SAP30. **F**, Distribution of BAHCC1, RBBP7, RBBP4, and SAP30 peaks in different regions of the human genome. **G**, IGV plots showing cooccupancy of BAHCC1, RBBP7, RBBP4, and SAP30 in the LMO7 gene transcription start site (TSS) region (boxed) in HAoSMCs. **H**, Enrichment of RBBP7, RBBP4, and SAP30 at LMO7 in HAoSMCs infected with LV-shRNA-SCR or LV-shRNA-BAHCC1, assessed by ChIP-qPCR. Quantification: 2-way ART ANOVA with Holm post hoc test (adjusted *P* values are shown on the graph), n=4 independent repeat experiments. **I**, Proliferation assay of HAoSMCs transfected with siRNA-Ctrl or siRNA-RBBP7, siRNA-RBBP4, or siRNA-SAP30, with or without FBS stimulation. Quantification: Kruskal-Wallis test with Benjamini-Krieger-Yekutieli post hoc correction (adjusted *P* values are shown on the graph); n=4 independent repeat experiments. **J**, IGV plots showing cooccupancy of BAHCC1, RBBP7, RBBP4, and SAP30 in the CDKN1B gene (P27) TSS region (boxed) in HAoSMCs. **K**, ChIP-qPCR indicating enrichment of BAHCC1 at P27 in HAoSMCs with or without PDGF-BB and enrichment of RBBP7, RBBP4, and SAP30 at P27 in HAoSMCs infected with LV-shRNA-SCR or LV-shRNA-BAHCC1. Quantification: 2-way ART ANOVA with Holm post hoc test (adjusted *P* values are shown on the graph); n=4 independent repeat experiments. All data are presented as mean ± SEM. TTS indicates transcription termination site; and UTR, untranslated region.

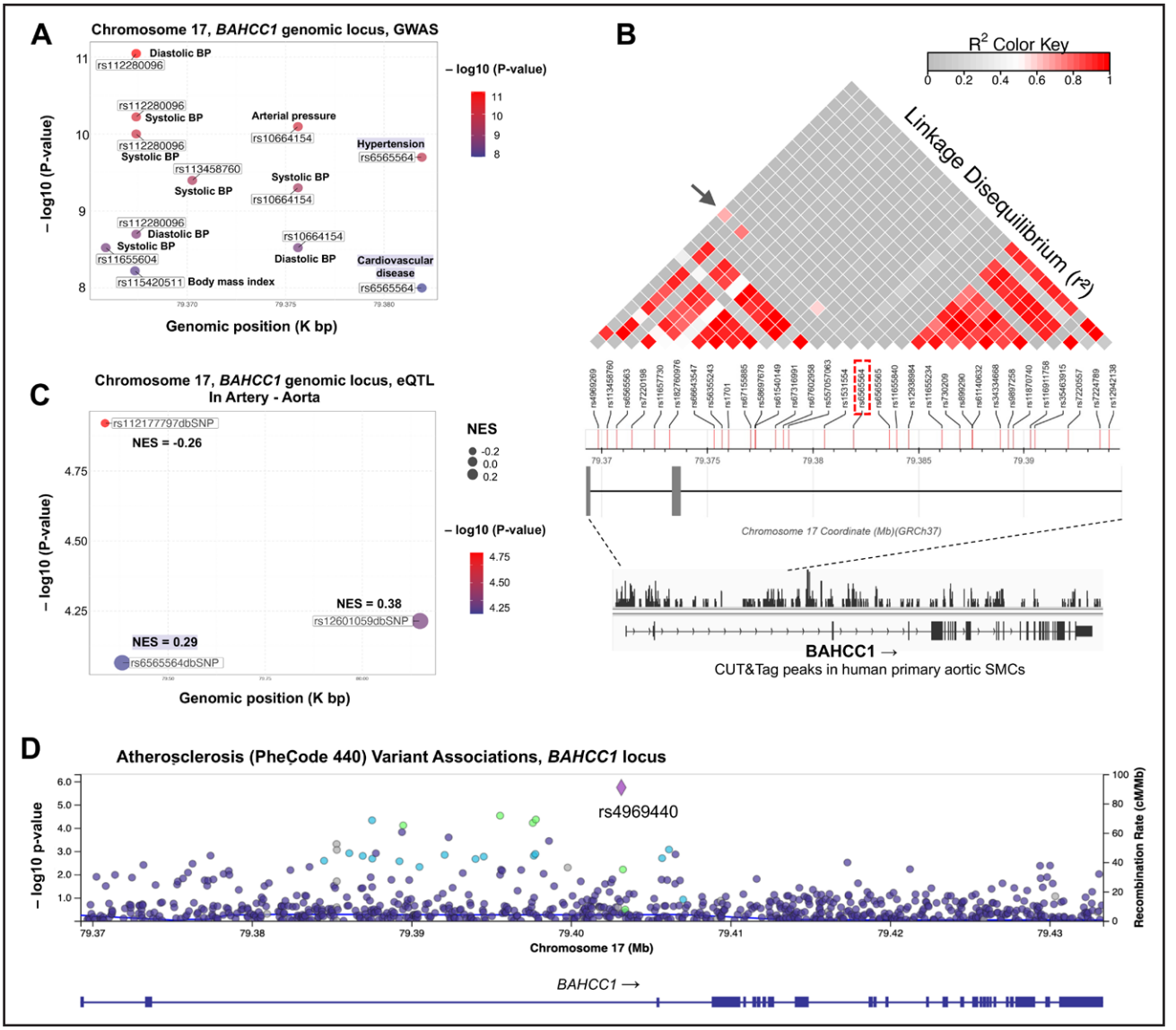


Figure 8. Association of BAHCC1 (bromo adjacent homology domain coiled-coil 1) genetic variation with human cardiovascular phenotypes.

A, *P* value plot showing genome-wide significant BAHCC1 variants that correlate with various cardiovascular phenotypes (labeled beside the variant numbers). **B**, Heatmap of pairwise linkage disequilibrium (LD) measurements for nearby BAHCC1 single nucleotide polymorphisms (SNPs) flanking rs6565564. Darker color indicates stronger correlation. Genomic locations of the SNPs surrounding rs6565564 are labeled, and correlated with the BAHCC1 CUT&Tag peaks at the *BAHCC1* locus. **C**, Expression quantitative trait loci (eQTL) plot. Normalized effect size (NES) values are indicated by circle size. *P* values are indicated by color. **D**, A BAHCC1 variant (rs4969440) from the Million Veteran Program meta-analysis showing a suggestive association with atherosclerosis (P=1.8×10^{-06}). BP indicates blood pressure.

ARTICLE INFORMATION

Received July 14, 2026; revision received October 15, 2026; accepted October 21, 2026.

Affiliations

Division of Surgical Sciences, Department of Surgery (R.T., Y.H., T.S., J.L., C.S., X.Z., J.M., K.C.K., L.-W.G.) and Department of Genome Sciences (G.A., P.H., M.M., C.L.M.), School of Medicine, University of Virginia, Charlottesville. Department of Biomedical Informatics, College of Medicine, The Ohio State University, Columbus (A.W.). Department of Biochemistry and Molecular Genetics (K.Z., J.Y.) and Department of Molecular Physiology and Biological Physics (L.-W.G.), University of Virginia, Charlottesville. Department of Pharmacology and Cancer Biology, Duke University School of Medicine, Durham, NC (Y.G., G.G.W.). Department of Medicine (Cardiovascular Medicine) (K.A.M.) and Department of Pharmacology (K.A.M.), Yale University School of Medicine, New Haven, CT. Robert M. Berne Cardiovascular Research Center, University of Virginia School of Medicine, Charlottesville (L.-W.G.).

Acknowledgments

The authors thank Dr Kenneth Walsh at the University of Virginia for helpful discussions.

Sources of Funding

This research was partially supported by National Institutes of Health awards R01HL168405 (to L.-W. Guo and K.C. Kent), R01HL133665 and R01HL171140 (to L.-W. Guo), R01HL177662 and R01HD110059 (to K.A. Martin), R01-CA268519 and R01-CA268384 (to G.G. Wang), and R01EY036243 and R01AG072430 (to J. Ma).

Downloaded from http://ahajournals.org by on November 5, 2026

Disclosures

None.

Supplemental Material

Expanded Materials & Methods
Figures S1–S21
Major Resources Tables
Uncropped Western Blots
References 59,60,61

REFERENCES

1. de Vries MR, Simons KH, Jukema JW, Braun J, Quax PH. Vein graft failure: from pathophysiology to clinical outcomes. *Nat Rev Cardiol*. 2016;13:451–470. doi: 10.1038/nrcardio.2016.76
2. Melnik T, Jordan O, Corpataux JM, Delie F, Saucy F. Pharmacological prevention of intimal hyperplasia: a state-of-the-art review. *Pharmacol Ther*. 2022;235:108157. doi: 10.1016/j.pharmthera.2022.108157
3. Hildick-Smith D, Behan MW, Lassen JF, Chieffo A, Lefevre T, Stankovic G, Burzotta F, Pan M, Ferenc M, Bennett L, et al. The EBC TWO Study (European Bifurcation Coronary TWO): a randomized comparison of provisional t-stenting versus a systematic 2 stent culotte strategy in large caliber true bifurcations. *Circ Cardiovasc Interv*. 2016;9:e003643. doi: 10.1161/CIRCINTERVENTIONS.115.003643
4. Madhavan MV, Kirtane AJ, Redfors B, Genereux P, Ben-Yehuda O, Palmerini T, Benedetto U, Biondi-Zoccai G, Smits PC, von Birgelen C, et al. Stent-related adverse events >1 year after percutaneous coronary intervention. *J Am Coll Cardiol*. 2020;75:590–604. doi: 10.1016/j.jacc.2019.11.058
5. Hofma SH, van der Giessen WJ, van Dalen BM, Lemos PA, McFadden EP, Sianos G, Ligthart JM, van Essen D, de Feyter PJ, Serruys PW. Indication of long-term endothelial dysfunction after sirolimus-eluting stent implantation. *Eur Heart J*. 2006;27:166–170. doi: 10.1093/eurheartj/ehi571
6. Valdes PJ, Akbar H, Kahloon RA, Diaz MA. Intracoronary Stents StatPearls Treasure Island (FL) ineligible companies. Disclosure: Hina Akbar declares no relevant financial relationships with ineligible companies. Disclosure: Rehan Kahloon declares no relevant financial relationships with ineligible companies. Disclosure: Miguel Diaz declares no relevant financial relationships with ineligible companies. 2025.
7. Wu W, Wang C, Zang H, Qi L, Azhar M, Nagarkatti M, Nagarkatti P, Cai G, Weiser-Evans MCM, Cui T. Mature vascular smooth muscle cells, but not endothelial cells, serve as the major cellular source of intimal hyperplasia in vein grafts. *Arterioscler Thromb Vasc Biol*. 2020;40:1870–1890. doi: 10.1161/ATVBAHA.120.314465
8. Chappell J, Harman JL, Narasimhan VM, Yu H, Foote K, Simons BD, Bennett MR, Jorgensen HF. Extensive Proliferation of a subset of differentiated, yet plastic, medial vascular smooth muscle cells contributes to neointimal formation in mouse injury and atherosclerosis models. *Circ Res*. 2016;119:1313–1323. doi: 10.1161/CIRCRESAHA.116.309799
9. Chakraborty R, Chatterjee P, Dave JM, Ostriker AC, Greif DM, Rzucidlo EM, Martin KA. Targeting smooth muscle cell phenotypic switching in vascular disease. *JVS Vasc Sci*. 2021;2:79–94. doi: 10.1016/j.jvssci.2021.04.001
10. Alexander MR, Owens GK. Epigenetic control of smooth muscle cell differentiation and phenotypic switching in vascular development and disease. *Annu Rev Physiol*. 2012;74:13–40. doi: 10.1146/annurev-physiol-012110-142315
11. Gomez D, Swiatlowska P, Owens GK. Epigenetic control of smooth muscle cell identity and lineage memory. *Arterioscler Thromb Vasc Biol*. 2015;35:2508–2516. doi: 10.1161/ATVBAHA.115.305044
12. Borck PC, Guo LW, Plutzky J. BET Epigenetic Reader Proteins in Cardiovascular Transcriptional Programs. *Circ Res*. 2020;126:1190–1208. doi: 10.1161/CIRCRESAHA.120.315929
13. Jiao L, Liu X. Structural basis of histone H3K27 trimethylation by an active polycomb repressive complex 2. *Science*. 2015;350:aac4383. doi: 10.1126/science.aac4383
14. Liu R, Jin Y, Tang WH, Qin L, Zhang X, Tellides G, Hwa J, Yu J, Martin KA. Ten-Eleven Translocation-2 (TET2) is a master regulator of smooth muscle cell plasticity. *Circulation*. 2013;128:2047–2057. doi: 10.1161/CIRCULATIONAHA.113.002887
15. Salmon M, Gomez D, Greene E, Shankman L, Owens GK. Cooperative binding of KLF4, pELK-1, and HDAC2 to a G/C repressor element in the SM22alpha promoter mediates transcriptional silencing during SMC phenotypic switching in vivo. *Circ Res*. 2012;111:685–696. doi: 10.1161/CIRCRESAHA.112.269811
16. Zhang M, Urabe G, Little C, Wang B, Kent AM, Huang Y, Kent KC, Guo LW. HDAC6 regulates the MRTF-A/SRF axis and vascular smooth muscle cell plasticity. *JACC Basic Transl Sci*. 2018;3:782–795. doi: 10.1016/j.jacbts.2018.08.010
17. Chakraborty R, Ostriker AC, Xie Y, Dave JM, Gamez-Mendez A, Chatterjee P, Abu Y, Valentine J, Lezon-Geyda K, Greif DM, et al. Histone acetyltransferases p300 and CBP coordinate distinct chromatin remodeling programs in vascular smooth muscle plasticity. *Circulation*. 2022;145:1720–1737. doi: 10.1161/CIRCULATIONAHA.121.057599
18. Liang J, Li Q, Cai W, Zhang X, Yang B, Li X, Jiang S, Tian S, Zhang K, Song H, et al. Inhibition of polycomb repressor complex 2 ameliorates neointimal hyperplasia by suppressing trimethylation of H3K27 in vascular smooth muscle cells. *Br J Pharmacol*. 2019;176:3206–3219. doi: 10.1111/bph.14754
19. Zhang M, Urabe G, Ozer HG, Xie X, Webb A, Shirasu T, Li J, Han R, Kent KC, Wang B, et al. Angioplasty induces epigenomic remodeling in injured arteries. *Life Sci Alliance*. 2022;5:e202101114. doi: 10.26508/lsa.202101114
20. Guo Y, Zhao S, Wang GG. Polycomb gene silencing mechanisms: PRC2 chromatin targeting, H3K27me3 'readout', and phase separation-based compaction. *Trends Genet*. 2021;37:547–565. doi: 10.1016/j.tig.2020.12.006
21. Fan H, Lu J, Guo Y, Li D, Zhang ZM, Tsai YH, Pi WC, Ahn JH, Gong W, Xiang Y, et al. BAHCC1 binds H3K27me3 via a conserved BAH module to mediate gene silencing and oncogenesis. *Nat Genet*. 2020;52:1384–1396. doi: 10.1038/s41588-020-00729-3
22. Berico P, Nogaret M, Cigrang M, Lallement A, Vand-Rajabpour F, Flores-Yanke A, Gambi G, Davidson G, Seno L, Obid J, et al. Super-enhancer-driven expression of BAHCC1 promotes melanoma cell proliferation and genome stability. *Cell Rep*. 2023;42:113363. doi: 10.1016/j.celrep.2023.113363
23. Zhang MW B, Urabe G, Shi X, Guo LW. Inhibition of the enhancer of zeste homolog family mitigates intimal hyperplasia in rat carotid arteries. *Arterioscler Thromb Vasc Biol*. 2017;37:A332–A332.
24. Deaton RA, Bulut G, Serbulea V, Salamon A, Shankman LS, Nguyen AT, Owens GK. A New Autosomal Myh11-CreER(T2) smooth muscle cell lineage tracing and gene knockout mouse model-brief report. *Arterioscler Thromb Vasc Biol*. 2023;43:203–211. doi: 10.1161/ATVBAHA.122.318160
25. Takayama T, Shi X, Wang B, Franco S, Zhou Y, DiRenzo D, Kent A, Hartig P, Zent J, Guo LW. A murine model of arterial restenosis: technical aspects of femoral wire injury. *J Vis Exp*. 2015. doi: 10.3791/52561-v
26. Buglak NE, Bahnson ESM. A rat carotid artery pressure-controlled segmental balloon injury with periadventitial therapeutic application. *J Vis Exp*. 2020. doi: 10.3791/60473
27. Wang B, Zhang M, Takayama T, Shi X, Roenneburg DA, Kent KC, Guo LW. BET bromodomain blockade mitigates intimal hyperplasia in rat carotid arteries. *EBioMedicine*. 2015;2:1650–1661. doi: 10.1016/j.ebiom.2015.09.045
28. Clowes AW, Reidy MA, Clowes MM. Mechanisms of stenosis after arterial injury. *Lab Invest*. 1983;49:208–215.
29. Xie Y, Ostriker AC, Jin Y, Hu H, Sizer AJ, Peng G, Morris AH, Ryu C, Herzog EL, Kyriakides T, et al. LMO7 is a negative feedback regulator of transforming growth factor beta signaling and fibrosis. *Circulation*. 2019;139:679–693. doi: 10.1161/CIRCULATIONAHA.118.034615
30. Li D, Zhang ZM, Mei L, Yu Y, Guo Y, Mackintosh SG, Chen J, Allison DF, Kim A, Storey AJ, et al. BAHCC1 binds H4K20me1 to facilitate the MCM complex loading and DNA replication. *Nat Commun*. 2025;16:5502. doi: 10.1038/s41467-025-61284-1
31. Monziani A, Perry RB, Hezroni H, Ulitsky I. BAHCC1 promotes gene expression in neuronal cells by antagonizing SIN3A-HDAC1. *Nucleic Acids Res*. 2025;53:gkaf650. doi: 10.1093/nar/gkaf650
32. Owens GK, Kumar MS, Wamhoff BR. Molecular regulation of vascular smooth muscle cell differentiation in development and disease. *Physiol Rev*. 2004;84:767–801. doi: 10.1152/physrev.00041.2003
33. Gomez D, Owens GK. Smooth muscle cell phenotypic switching in atherosclerosis. *Cardiovasc Res*. 2012;95:156–164. doi: 10.1093/cvr/cvs115
34. Spin JM, Maegdefessel L, Tsao PS. Vascular smooth muscle cell phenotypic plasticity: focus on chromatin remodelling. *Cardiovasc Res*. 2012;95:147–155. doi: 10.1093/cvr/cvs098
35. Silvestre-Roig C, Fernandez P, Esteban V, Pello OM, Indolfi C, Rodriguez C, Rodriguez-Calvo R, Lopez-Maderuelo MD, Bauriedel G, Hutter R, et al. Inactivation of nuclear factor-Y inhibits vascular smooth muscle cell proliferation and neointima formation. *Arterioscler Thromb Vasc Biol*. 2013;33:1036–1045. doi: 10.1161/ATVBAHA.112.300580
36. Szklarczyk D, Morris JH, Cook H, Kuhn M, Wyder S, Simonovic M, Santos A, Doncheva NT, Roth A, Bork P, et al. The STRING database in 2017: quality-controlled protein-protein association networks, made broadly accessible. *Nucleic Acids Res*. 2017;45:D362–D368. doi: 10.1093/nar/gkw937

Downloaded from http://ahajournals.org by on November 5, 2026

Circulation Research
FIRST PROOF ONLY

37. Abramson J, Adler J, Dunger J, Evans R, Green T, Pritzel A, Ronneberger O, Willmore L, Ballard AJ, Bambrick J, et al. Accurate structure prediction of biomolecular interactions with AlphaFold 3. *Nature*. 2024;630:493–500. doi: 10.1038/s41586-024-07487-w
38. Pichler K, Warner K, Magrane M, UniProt C. SPIN: Submitting sequences determined at protein level to UniProt. *Curr Protoc Bioinformatics*. 2018;62:e52. doi: 10.1002/cpbi.52
39. Laugesen A, Helin K. Chromatin repressive complexes in stem cells, development, and cancer. *Cell Stem Cell*. 2014;14:735–751. doi: 10.1016/j.stem.2014.05.006
40. Kichaev G, Bhatia G, Loh PR, Gazal S, Burch K, Freund MK, Schoech A, Pasaniuc B, Price AL. Leveraging polygenic functional enrichment to improve GWAS power. *Am J Hum Genet*. 2019;104:65–75. doi: 10.1016/j.ajhg.2018.11.008
41. Carey CE, Shafee R, Wedow R, Elliott A, Palmer DS, Compitello J, Kanai M, Abbott L, Schultz P, Karczewski KJ, et al. Principled distillation of UK Biobank phenotype data reveals underlying structure in human variation. *Nat Hum Behav*. 2024;8:1599–1615. doi: 10.1038/s41562-024-01909-5
42. Verma A, Huffman JE, Rodriguez A, Conery M, Liu M, Ho YL, Kim Y, Heise DA, Guare L, Panickan VA, et al. Diversity and scale: genetic architecture of 2068 traits in the VA million veteran program. *Science*. 2024;385:eadj1182. doi: 10.1126/science.adj1182
43. Zhuang J, Luan P, Li H, Wang K, Zhang P, Xu Y, Peng W. The Yin-Yang dynamics of DNA methylation is the key regulator for smooth muscle cell phenotype switch and vascular remodeling. *Arterioscler Thromb Vasc Biol*. 2017;37:84–97. doi: 10.1161/ATVBAHA.116.307923
44. Chatterjee P, Chakraborty R, Sizer AJ, O'Brien BJ, Xu P, Hwa JM, Xie Y, Yan Q, Hwa J, Martin KA. SUV39H1 regulates KLF4 and chromatin remodeling in smooth muscle cell phenotypic plasticity. *Arterioscler Thromb Vasc Biol*. 2025;45:2015–2033. doi: 10.1161/ATVBAHA.124.322179
45. Yang Y, Zhang Q, Liu S, Yuan H, Wu X, Zou Y, Zhang Y, Guo J. Suv39h1 regulates phenotypic modulation of smooth muscle cells and contributes to vascular injury by repressing HIC1 transcription. *Arterioscler Thromb Vasc Biol*. 2025;45:965–978. doi: 10.1161/ATVBAHA.124.322048
46. Shirasu T, Urabe G, Yodsanit N, Huang Y, Xie R, Stratton MS, Joseph M, Zhang Z, Wang Y, Li J, et al. Nano-based perivascular intervention sustains a nine-month long-term suppression of intimal hyperplasia in vein grafts. *Bioact Mater*. 2025;44:82–96. doi: 10.1016/j.bioactmat.2024.10.005
47. Zhang J, Chen J, Yang J, Xu C, Hu Q, Wu H, Cai W, Guo Q, Gao W, He C, et al. Suv39h1 downregulation inhibits neointimal hyperplasia after vascular injury. *Atherosclerosis*. 2019;288:76–84. doi: 10.1016/j.atherosclerosis.2019.06.909
48. Guo J, Qiu J, Jia M, Li Q, Wei X, Li L, Pan Q, Jin J, Ge F, Ma S, et al. BACH1 deficiency prevents neointima formation and maintains the differentiated phenotype of vascular smooth muscle cells by regulating chromatin accessibility. *Nucleic Acids Res*. 2023;51:4284–4301. doi: 10.1093/nar/gkad120
49. Nakamura A, Masuya M, Shinmei M, Tawara I, Nosaka T, Ono R. Bahcc1 is critical for the aberrant epigenetic program in a mouse model of MLL-ENL-mediated leukemia. *Blood Adv*. 2024;8:2193–2206. doi: 10.1182/bloodadvances.2023011320
50. Hezroni H, Ben-Tov Perry R, Gil N, Degani N, Ulitsky I. Regulation of neuronal commitment in mouse embryonic stem cells by the Reno1/Bahcc1 locus. *EMBO Rep*. 2020;21:e51264. doi: 10.15252/embr.202051264
51. Li J, Shen H, Guo LW. Transmembrane protein TMEM97 and epigenetic reader BAHCC1 constitute an axis that supports pro-inflammatory cytokine expression. *Cell Signal*. 2024;116:111069. doi: 10.1016/j.cellsig.2024.111069
52. Zhang M, Li J, Wang Q, Urabe G, Tang R, Huang Y, Mosquera JV, Kent KC, Wang B, Miller CL, et al. Gene-repressing epigenetic reader EED unexpectedly enhances cyclinD1 gene activation. *Mol Ther Nucleic Acids*. 2023;31:717–729. doi: 10.1016/j.omtn.2023.02.024
53. Cheong A, Bingham AJ, Li J, Kumar B, Sukumar P, Munsch C, Buckley NJ, Neylon CB, Porter KE, Beech DJ, et al. Downregulated REST transcription factor is a switch enabling critical potassium channel expression and cell proliferation. *Mol Cell*. 2005;20:45–52. doi: 10.1016/j.molcel.2005.08.030
54. Zhang Y, Sun ZW, Iratni R, Erdjument-Bromage H, Tempst P, Hampsey M, Reinberg D. SAP30, a novel protein conserved between human and yeast, is a component of a histone deacetylase complex. *Mol Cell*. 1998;1:1021–1031. doi: 10.1016/s1097-2765(00)80102-1
55. Streubel G, Fitzpatrick DJ, Oliviero G, Scelfo A, Moran B, Das S, Munawar N, Watson A, Wynne K, Negri GL, et al. Fam60a defines a variant Sin3a-Hdac complex in embryonic stem cells required for self-renewal. *EMBO J*. 2017;36:2216–2232. doi: 10.15252/embj.201696307
56. Cai Y, Zhang Y, Loh YP, Tng JQ, Lim MC, Cao Z, Raju A, Lieberman Aiden E, Li S, Manikandan L, et al. H3K27me3-rich genomic regions can function as silencers to repress gene expression via chromatin interactions. *Nat Commun*. 2021;12:719. doi: 10.1038/s41467-021-20940-y
57. Mohd-Sarip A, Cleard F, Mishra RK, Karch F, Verrijzer CP. Synergistic recognition of an epigenetic DNA element by Pleiohomeotic and a Polycomb core complex. *Genes Dev*. 2005;19:1755–1760. doi: 10.1101/gad.347005
58. Vahed SZ, Khatibi SMH, Saadat YR, Emdadi M, Khodaei B, Alishani MM, Boostani F, Dizaj SM, Pirmoradi S. Introducing effective genes in lymph node metastasis of breast cancer patients using SHAP values based on the mRNA expression data. *PLoS One*. 2024;19:e0308531. doi: 10.1371/journal.pone.0308531
59. Shirasu T, Yodsanit N, Li J, Huang Y, Xie X, Tang R, Wang Q, Zhang M, Urabe G, Webb A, et al. Neointima abating and endothelium preserving—an adventitia-localized nanoformulation to inhibit the epigenetic writer DOT1L. *Biomaterials*. 2023;301:122245. doi: 10.1016/j.biomaterials.2023.122245
60. Huang Y, Urabe G, Zhang M, Li J, Ozer HG, Wang B, Kent KC, Guo LW. Nullifying epigenetic writer DOT1L attenuates neointimal hyperplasia. *Atherosclerosis*. 2020;308:22–31. doi: 10.1016/j.atherosclerosis.2020.06.002
61. Zhang Y, Liu T, Meyer CA, Eeckhoute J, Johnson DS, Bernstein BE, Nusbaum C, Myers RM, Brown M, Li W, et al. Model-based analysis of ChIP-Seq (MACS). *Genome Biol*. 2008;9:R137. doi: 10.1186/gb-2008-9-9-r137

Downloaded from http://ahajournals.org by on November 5, 2026

Circulation Research
NOT PROOFREAD